

SANDIA REPORT

SAND84-1697 • UC-70

Unlimited Release

Printed September 1988

Nevada Nuclear Waste Storage Investigations Project

Capillary-Driven Flow in a Fracture Located in a Porous Medium

Mario J. Martinez

Prepared by
Sandia National Laboratories
Albuquerque, New Mexico 87185 and Livermore, California 94550
for the United States Department of Energy
under Contract DE-AC04-76DP00789

HYDROLOGY DOCUMENT NUMBER 371

"Prepared by Nevada Nuclear Waste Storage Investigations (NNWSI) Project participants as part of the Civilian Radioactive Waste Management Program (CRWM). The NNWSI Project is managed by the Waste Management Project Office (WMPO) of the U.S. Department of Energy, Nevada Operations Office (DOE/NV). NNWSI Project work is sponsored by the Office of Geologic Repositories (OGR) of the DOE Office of Civilian Radioactive Waste Management (OCRWM)."

Issued by Sandia National Laboratories, operated for the United States Department of Energy by Sandia Corporation.

NOTICE: This report was prepared as an account of work sponsored by an agency of the United States Government. Neither the United States Government nor any agency thereof, nor any of their employees, nor any of their contractors, subcontractors, or their employees, makes any warranty, express or implied, or assumes any legal liability or responsibility for the accuracy, completeness, or usefulness of any information, apparatus, product or process disclosed, or represents that its use would not infringe privately owned rights. Reference herein to any specific commercial product, process, or service by trade name, trademark, manufacturer, or otherwise, does not necessarily constitute or imply its endorsement, recommendation, or favoring by the United States Government, any agency thereof or any of their contractors or subcontractors. The views and opinions expressed herein do not necessarily state or reflect those of the United States Government, any agency thereof or any of their contractors.

Printed in the United States of America
Available from
National Technical Information Service
U.S. Department of Commerce
5285 Port Royal Road
Springfield, VA 22161

NTIS price codes
Printed copy: A04
Microfiche copy: A01

Distribution
Category UC-70

SAND84-1697
Unlimited Release
Printed September 1988

CAPILLARY-DRIVEN FLOW IN A FRACTURE LOCATED IN A POROUS MEDIUM

Mario J. Martinez
Fluid Mechanics and Heat Transfer Division I
Sandia National Laboratories
Albuquerque, NM 87185

ABSTRACT

Capillary-driven immiscible displacement of air by water along an isolated fracture located in a permeable medium is induced by an abrupt change in water saturation at the fracture inlet. The fracture is idealized as either a smooth slot with permeable walls or a high-permeability layer. The penetration distance of moisture in the fracture is shown to depend on the square root of matrix to fracture permeability ratio and length scales for the problem. The models are applied to materials representative of the Yucca Mountain region of the Nevada Test Site. Fracture moisture-penetration histories are predicted for several units in Yucca Mountain and for representative fracture apertures.

CONTENTS

	Page
INTRODUCTION	1
GOVERNING EQUATIONS	5
Field Equations	5
Material Models	6
Initial and Boundary Conditions	10
ANALYSIS	11
Flow in the Porous Matrix	11
Flow in a Permeable-Walled Slot	12
Flow in a Sandy Fracture	14
APPLICATION TO YUCCA MOUNTAIN	16
Material Properties for Yucca Mountain	16
Flow in Yucca Mountain Materials	16
Flow in the Fracture	17
SUMMARY	40
REFERENCES	41
APPENDIX A	43
APPENDIX B	44

FIGURES

<u>Figure</u>		<u>Page</u>
1	Schematic of moisture penetration in a vertical fracture located in a permeable matrix	3
2	Hypothetical capillary and relative permeability curves	8
3	Effective material curves for a smooth slot	9
4	Material properties for the Calico Hills nonwelded vitric unit (from Peters and Gauthier)	18
5	Material properties for the Topopah Spring welded unit (from Peters and Gauthier)	19
6	Material properties for the Paintbrush nonwelded unit (from Peters and Gauthier)	20
7	Material properties for the Tiva Canyon welded unit (from Peters and Gauthier)	21
8	Pressure head distribution in the Calico Hills nonwelded (vitric) unit	22
9	Pressure head distribution in the Topopah Spring welded unit	23
10	Pressure head distribution in the Paintbrush nonwelded unit	24
11	Pressure head distribution in the Tiva Canyon welded unit	25
12	Variation of fracture moisture penetration with loss parameter f	27
13	Moisture penetration for a 25 μm fracture located in an impermeable matrix ($f=0$), the Tiva Canyon (1.59) and the Topopah Spring (4.66)	30
14	Pressure head and saturation distributions in a 25 μm fracture embedded in an impermeable matrix	32
15	Hydraulic conductivity and Darcy flux distributions in a 25 μm fracture embedded in an impermeable matrix	33
16	Pressure head and saturation distributions in a 25 μm fracture located in the Topopah Spring welded unit	34

	<u>Page</u>
17 Hydraulic conductivity and saturation distributions in a 25 μm fracture located in the Topopah Spring welded unit	35
18 Pressure head and saturation distributions in a 25 μm fracture located in the Tiva Canyon welded unit	36
19 Hydraulic conductivity and Darcy flux distributions in a 25 μm fracture located in the Tiva Canyon welded unit	37
20 Moisture penetration for a 100 μm fracture as given by the smooth slot model. The matrix material is impermeable ($f=0$), the Tiva Canyon (0.10), and the Topopah Spring (0.29)	39

TABLES

	<u>Page</u>
1. Matrix Properties for Yucca Mountain	17
2. Boundary Gradient from Matrix Flow Solutions	26
3. Loss Parameters for Smooth Slot Fracture Model for Calico Hills Nonwelded	28
4. Loss Parameters for Smooth Slot Fracture Model for Topopah Spring	28
5. Loss Parameters for Smooth Slot Fracture Model for Paintbrush	29
6. Loss Parameters for Smooth Slot Fracture Model for Tiva Canyon	29

NOTATION

a	- fit parameter for matrix material functions, (1/L)
b	- fit parameter for matrix material functions
c	- (=1-1/b)
C	- material capacitance function (Eqns. (13), (25))
f	- dimensionless seepage loss parameter
g	- gravity, (L/T ²)
h	- hydraulic head, (L)
H	- dimensionless head (Eqn. (25))
k	- permeability, (L ²)
k _r	- relative permeability, (k _r (ψ) or k _r (h))
K	- saturated conductivity (K _f = k _f ρg/μ , K _m = k _m ρg/μ)
L	- dimensionless penetration, (L = l/ψ _c)
P	- normalized pressure head, (P = -aψ)
q	- dimensionless loss parameter (Eqn. (27))
Q	- lateral seepage loss term (Eqn. (17))
R	- matrix-fracture diffusivity ratio (Eqn. (13))
s	- moisture saturation
t	- time, (T)
u	- Darcy flux in fracture, (L/T)
v	- Darcy flux in matrix, (L/T)
w	- fracture aperture, (L)
x,y	- spatial coordinates, (L)

Greek Symbols

B	- dimensionless pressure ratio, (Eqn. (15))
η	- similarity variable, (Eqn. (15))
θ	- moisture content
μ	- fluid viscosity, (M/LT)
ρ	- fluid density, (M/L ³)
σ	- surface tension, (M/T ²), (σ = 7.3 x 10 ⁻² N/m air-water)

- τ - dimensionless time ($\tau = K_f t / \psi_c$)
- x - moisture penetration distance in fracture, (L)
- ψ - pressure head
- $\Delta\theta$ - moisture difference ($\Delta\theta_f = \theta_{sf} - \theta_{rf}$; $\Delta\theta_m = \theta_{sm} - \theta_{rm}$)
- $\Delta\psi$ - pressure head difference ($\Delta\psi = \psi_o - \psi_\infty$)

Subscripts/Superscripts

- c - refers to capillary pressure head
- f,m - fracture or matrix
- s - slot, saturated value
- r - residual
- o,∞ - fracture inlet, far field or initial
- sf,sm - saturated value for fracture or matrix
- rf,rm - relative value for fracture or matrix
- $*,+$ - normalized quantity

ACKNOWLEDGMENT

R. R. Peters, Sandia National Laboratories, and J. Gauthier, Spectra Research, Inc., provided the plots of material property data for Yucca Mountain. Discussions with S. K. Griffiths and M. R. Bear of Sandia National Laboratories concerning scaling and the method of lines technique, respectively, are especially appreciated.

INTRODUCTION

The Yucca Mountain* region of the Nevada Test Site has been identified as a potential nuclear waste repository site. Fractures and faults are present in much of the mountain, as is characteristic of geological materials. The fracturing raises questions regarding the containment capabilities of a repository sited in such a material, since contaminant transport to the biosphere by groundwater is a scenario that will be studied as part of the assessment of the repository performance. Considerable attention has been given to describing mass transport in saturated fractured porous materials,¹⁻⁴ but very little work has been directed to the same phenomena in the unsaturated zone. Candidate repository horizons at Yucca Mountain lie above the water table. While the fracture network provides the primary path for flow in the saturated region, this may not be the case in the unsaturated zone. Capillary forces are the dominant mechanism for moisture transport in unsaturated porous materials. Regions of small characteristic pore size in an inhomogeneous porous medium have the highest propensity to absorb and retain moisture. The capillary force manifests itself as a pressure jump across the curved interface between two immiscible fluids (e.g., air-water in the present study). The magnitude of the pressure discontinuity (capillary force) is inversely proportional to the local radius of curvature of the interface and so increases as the characteristic pore size of the medium decreases. One would infer that flow in an unsaturated fractured medium is matrix dominated because of the rapid desaturation of large pore regions (fracture space) in comparison with the small pore regions of the intact rock.

The local moisture content must be near saturation before fracture permeabilities exceed those of the intact rock. However, geologic sources of infiltration are episodic and of short duration, giving rise to locally saturated regions. Thus, significant transport may occur during short

*The Nevada Nuclear Waste Storage Investigations (NNWSI) Project, managed by the Nevada Operations Office of the U.S. Department of Energy, is examining the feasibility of siting a repository for high-level nuclear wastes at Yucca Mountain on and adjacent to the Nevada Test Site. This work was funded in part by the NNWSI Project. The ultimate use of this information will be for system analysis and performance assessment of a nuclear waste repository in tuff.

infiltration periods through the high-permeability flow paths created by saturating the fracture network.

This analysis considers the dynamics of capillary-driven immiscible displacement of air by water in an isolated fracture embedded in a permeable matrix, Figure 1. Flow is induced in the fracture by an abrupt increase in moisture content to saturation at the fracture inlet. The fracture is analyzed as either a smooth capillary slot or a high-permeability slot filled with a coarse (relative to the surrounding matrix) material characteristic of sand or soil. The flow in the fracture is one-dimensional with lateral seepage losses to the matrix accounted for by a source term in the mass balance equation. The form of the source term is derived by considering the flow in the intact matrix. The analysis provides quantities of engineering interest such as the penetration length of moisture in the fracture, the flux of moisture transported by the fracture, and the dependence of the fracture seepage loss term on system parameters.

Because of the large contrast between fracture and matrix permeability, the fluid flow in the matrix is considered one-dimensional in a direction locally perpendicular to the fracture plane. The one-dimensional nonlinear diffusion problem admits the usual similarity transformation and is solved by a shooting technique for various materials representative of Yucca Mountain.

An approximate solution is derived when the fracture is idealized as a smooth slot with permeable walls. A one-parameter, integro-differential equation describes the location of the moisture front in the fracture. The parameter in the equation represents the lateral seepage losses in nondimensional form. The equation can be solved numerically for various representative loss parameters, resulting in penetration lengths as a function of time. Pressure head and flux distributions can also be determined as functions of the penetration length solution.

When the fracture is assumed to possess a pore structure, which is approximated by considering it to be filled with a coarse material, the resulting partial differential equation is solved numerically by the method of lines.⁵ Capillary curves for the fill material are assumed to be similar to those for sand or soil. Nondimensionalization of the governing

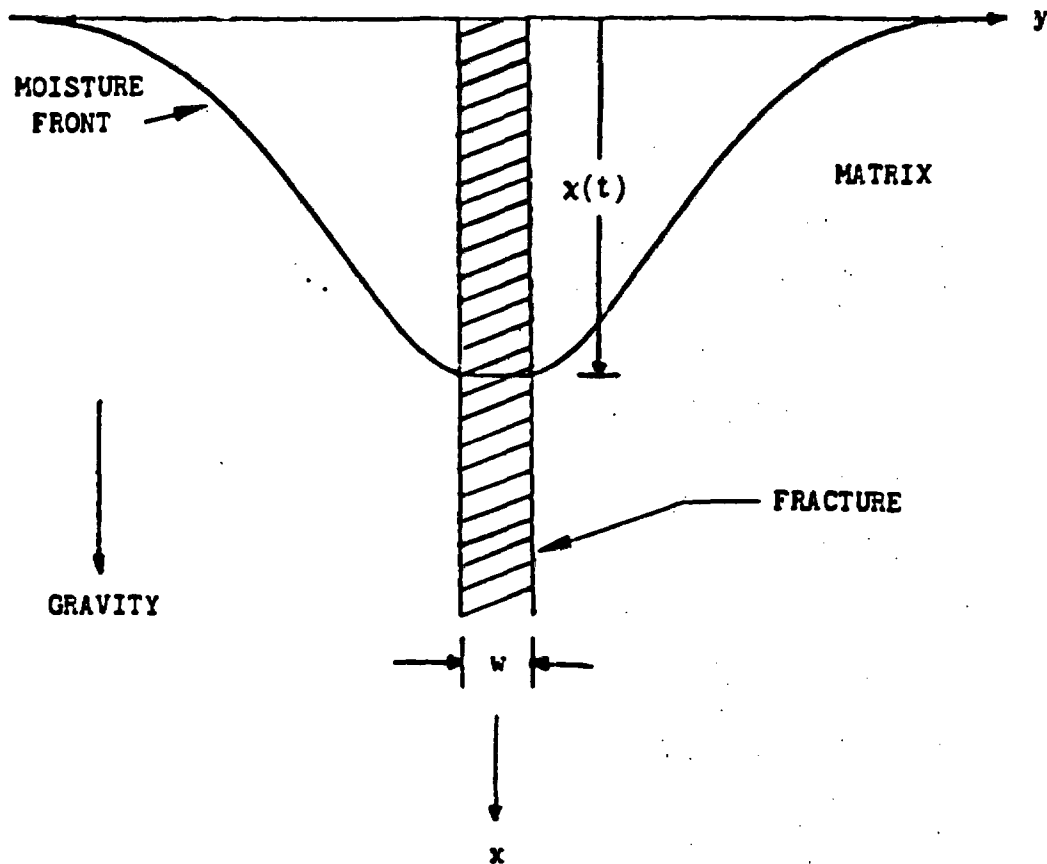


Figure 1. Schematic of moisture penetration in a vertical fracture located in a permeable matrix.

equations also produces a loss parameter of the same form found for the idealized slot case. Comparison of solutions for the two approaches results in similar fracture moisture-penetration histories.

GOVERNING EQUATIONS

Field Equations

One-dimensional flow of an incompressible fluid in a fracture embedded in less permeable material is described by the balance of mass and momentum:

$$\frac{\partial \theta_f}{\partial t} + \frac{\partial u}{\partial x} + \frac{2v_w}{w} = 0 \quad (1)$$

$$u = - \frac{\rho g}{\mu} k_f \frac{\partial h}{\partial x}, \quad h = \psi - x \quad (2)$$

where θ_f is moisture content, u is Darcy flux along the fracture, v_w is the seepage loss to the permeable material, w is the fracture aperture, h is the hydraulic head, ψ is the pressure head, and $k_f = k_{sf} k_{rf}$ is the permeability, which is the product of saturated (k_{sf}) and relative (k_{rf}) permeabilities. Darcy flow is assumed to predominate in the fracture as stated in the reduced momentum equation (2). The saturated permeability is given by

$$k_{sf} = \frac{w^2}{12} \quad (3)$$

which is derived from analysis of laminar flow in a slot and has also been shown to hold for saturated natural fractures.⁶ The source term v_w accounts for the seepage loss from the fracture to the surrounding matrix. The loss term is determined by resolving the flow in the intact rock matrix region.

Two-dimensional fluid flow in the matrix is also governed by the balance of mass and momentum:

$$\frac{\partial \theta_m}{\partial t} + \nabla \cdot \underline{v} = 0 \quad (4)$$

$$\underline{v} = - \frac{\rho g}{\mu} k_m \nabla h \quad (5)$$

where θ_m and k_m are the moisture content and permeability, respectively, in the matrix. Darcy flow is also assumed to hold for the matrix region.

Requiring continuity of the mass exchange between the fracture and matrix, from (5), the loss term for the fracture is given by

$$v_w = - \frac{\rho g}{\mu} k_{sm} \left. \frac{\partial h}{\partial y} \right|_{y=w/2} \quad (6)$$

Material Models

Because the problem domain lies above the water table, relative permeability and moisture content are functions of the liquid saturation. Neglecting the hysteresis in these functions associated with the imbibition or drainage of a porous material, we assume a unique functional relation between the moisture content and capillary pressure and also between relative permeability and liquid saturation. The former is usually referred to as the capillary or characteristic curve for the particular material under consideration. In view of the fact that liquid saturation is the moisture content scaled by the porosity, the relative permeability is a unique function of capillary pressure. We also note that, in neglecting balance equations for the gaseous (air in this case) phase, we have invoked the approximation that the gaseous phase is free to move without impeding the flow of liquid. This approximation is common in the soil physics literature and entails approximating the gas phase pressure as constant for all time. The approximation is adequate for high-permeability materials; however, its use for low-permeability materials is not as easily justified. Taking the gas phase pressure as atmospheric, the liquid pressure head, which we will simply refer to as pressure head in the remainder of this report, is the negative of the capillary pressure head.

Although we are unaware of any data on the capillary characteristics of in situ fractures, we approximate their behavior following the discussion of the role of capillary forces in the transport of moisture presented in the introduction. As the pressure head decreases (i.e., as capillary pressure increases) from its value at saturation, desaturation of liquid occurs first in the large pores of a porous material. The smaller pores, which can maintain smaller radii of curvature across the fluid interface, require a much lower pressure head before desaturation will commence. Hence, the pore size distribution of a porous material is important in determining the moisture content/capillary pressure relationship for the material. A

coarsely graded material (i.e., a material with a narrow band of pore size) will exhibit a rapidly varying capillary curve with abrupt transition from saturation to residual moisture content. This effect is illustrated in the schematic of capillary and relative permeability curves for poorly-graded and well-graded materials shown in Figure 2. Here we make the approximation that fractures, being a region of large characteristic pore size relative to the intact rock, are of the poorly graded material type and will exhibit strongly bimodal behavior. If we further idealize the fracture as a smooth slot, "effective" capillary and relative permeability curves will exhibit a step function transition from saturated to residual values. This idealization is depicted in Figure 3. The value of capillary pressure head at the step will be given by

$$\psi_c = \frac{2\sigma \cos \alpha}{\rho g w} \quad (7)$$

where σ is the surface tension between the two fluids, α is the contact angle and w is the aperture of the slot. Equation (7) is the capillary rise equation for a slot where the air phase pressure is atmospheric. Any pressure head less than $-\psi_c$ will result in desaturation of the slot.

Capillary and relative permeability data for the matrix region can be obtained experimentally. However, measurement of the relative permeability is especially difficult because of the small values typical of crystalline materials for which the present analysis is most applicable. A general set of functional forms is assumed to adequately describe the matrix material curves. Data for moisture content as a function of pressure head may be fit to the functions investigated by van Genuchten,⁷ which are of the following form

$$\frac{\theta - \theta_r}{\theta_s - \theta_r} = \left(\frac{1}{1 + P^b} \right)^c, \quad c = 1 - 1/b \quad (8)$$

where $P = -a\psi$ is the normalized capillary pressure in which the air phase pressure is assumed atmospheric, θ , θ_s , and θ_r are moisture content, connected porosity, and residual moisture content, respectively. The fit

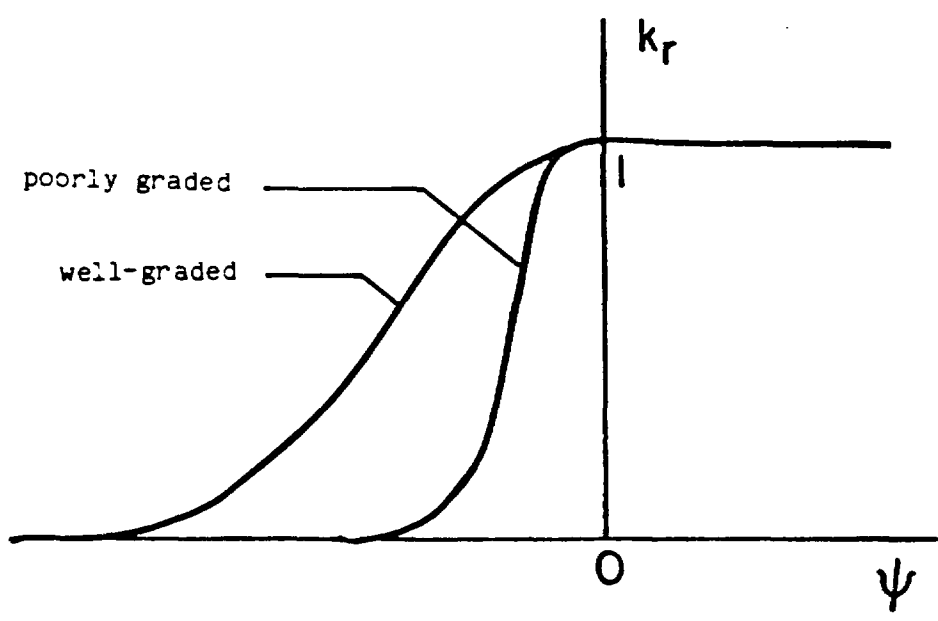
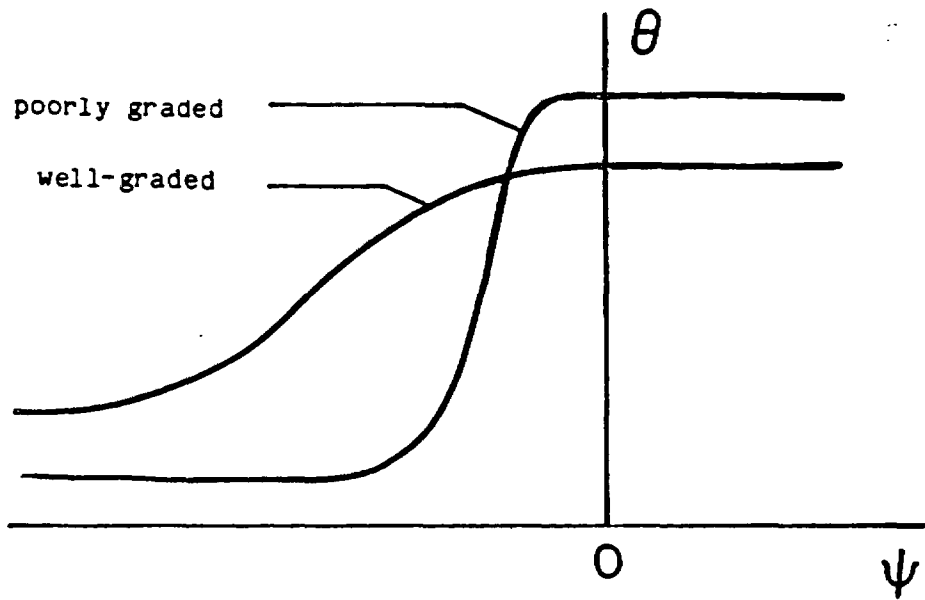
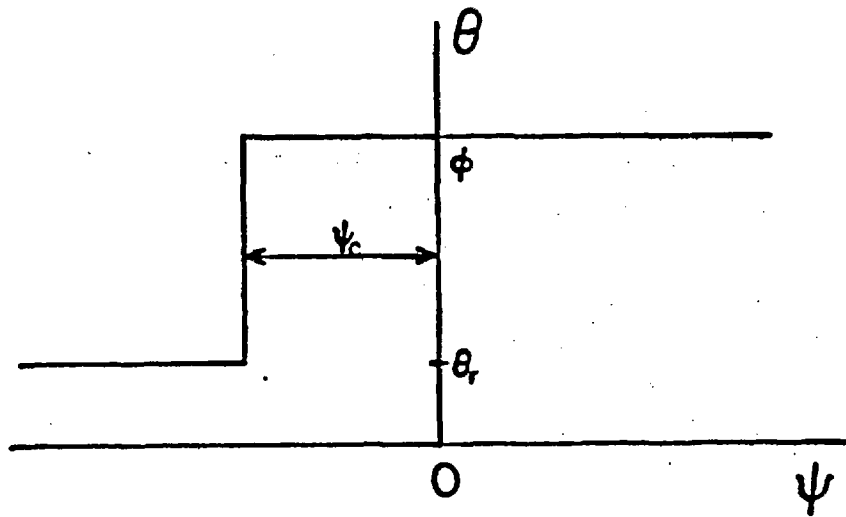
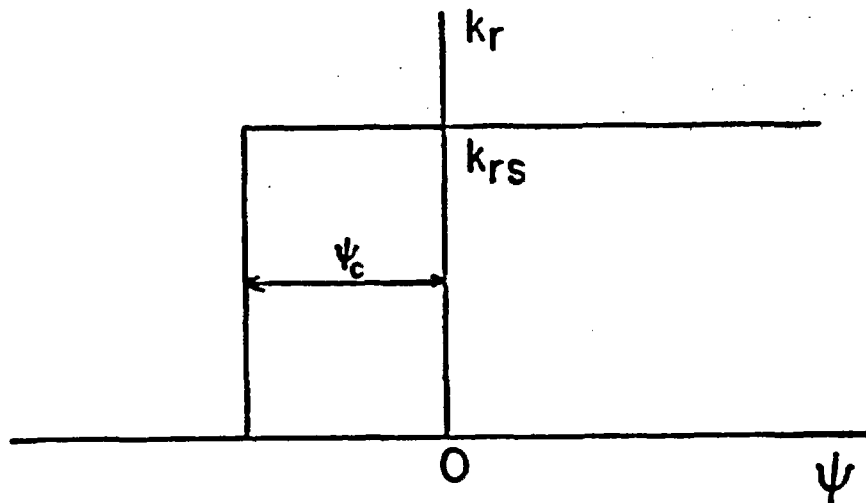


Figure 2. Hypothetical capillary and relative permeability curves.



a) Capillary curve



b) Relative permeability

Figure 3. Effective material curves for a smooth slot.

parameters, a and b , are related to the characteristic pressure head and steepness of the function, respectively. The moisture capacitance is given by differentiation of the capillary curve resulting in

$$\frac{d\theta}{d\psi} = a(b-1)(\theta_s - \theta_r) \frac{p^{b-1}}{(1+p^b)^{c+1}} \quad (9)$$

The relative permeability as a function of pressure head is assumed to be adequately described by the theory of Mualem⁸ which gives

$$k_r = \left(1 - \left(\frac{p^b}{1+p^b}\right)^c\right)^2 \left(\frac{1}{1+p^b}\right)^{c/2}, \quad c = 1 - 1/b$$

$$P = -a\psi \quad (10)$$

The parameters a and b in (10) are the same as in (8) and (9). Mualem's theory has shown good agreement with soil data.

Initial and Boundary Conditions

The specification of initial and boundary conditions completes the statement of the problem. Initially, the pressure head (and saturation) is constant, so the hydraulic head is given by

$$h(x,y,0) = h_\infty = \psi_\infty - x \quad (11a)$$

The flow in the fracture is induced by an abrupt change in saturation at the inlet

$$h(0,y,t) = h_0 = \psi_0 \quad (11b)$$

ANALYSIS

Flow in the Porous Matrix

The infiltration source for the present problem is episodic, appropriately simulating precipitation. Furthermore, the ratio of matrix to fracture permeability is taken to be small, and thus the penetration distance of moisture into the matrix is assumed to be less than the half-spacing between fractures. Under these assumptions the problem is semi-infinite for times of interest. Length scales for the problem are provided by the fracture aperture, w , and the moisture diffusivities⁹

$$\frac{\rho g}{\mu} k_{si} k_{ri} \left/ \frac{d\theta_i}{d\psi} \right., \quad i = f \text{ or } m$$

which suggest the following dimensionless variables¹⁰

$$\begin{aligned} \psi^* &= \frac{\psi - \psi_\infty}{\psi_0 - \psi_\infty}, & t^* &= \frac{t}{w^2} \frac{K_f}{\Delta\theta_f / \Delta\psi} \\ x^* &= x/w, & y^* &= \frac{y - w/2}{w} \sqrt{\frac{K_f}{K_m} \frac{\Delta\theta_m}{\Delta\theta_f}} = \frac{y - w/2}{w} \frac{1}{\sqrt{R}} \end{aligned} \quad (12)$$

where $K_f / (\Delta\theta_f / \Delta\psi)$ and $K_m / (\Delta\theta_m / \Delta\psi)$ are nominal measures of the diffusivity for the fracture and matrix. The transverse coordinate, y , is scaled to reflect the large longitudinal-to-transverse advance ratio of moisture, and the time scale acknowledges that the fracture is the dominant flow path as suggested by Nilson.¹⁰ In the scaled coordinates, the combination of (4) and (5) reads

$$C_m(\psi^*) \frac{\partial \psi^*}{\partial t^*} = R \frac{\partial}{\partial x^*} \left[k_{rm} \left(\frac{\partial \psi^*}{\partial x^*} - \frac{w}{\Delta\psi} \right) \right] + \frac{\partial}{\partial y^*} \left[k_{rm} \frac{\partial \psi^*}{\partial y^*} \right] \quad (13)$$

where

$$C_m(P(\psi^*)) = \frac{P^{b_m - 1}}{(1 + P^{b_m})^{c_m + 1}}, \quad R = \frac{K_m}{K_f} \frac{\Delta\theta_f}{\Delta\theta_m}$$

Since $R \ll 1$ in the present problem, the flow in the matrix is governed by the one-dimensional nonlinear diffusion equation, which admits the usual

similarity transformation $\eta = y/\sqrt{t}$. In these coordinates, the matrix equation (13) is rewritten as

$$\frac{d}{d\eta} \left(k_{rm} \frac{d\psi^*}{d\eta} \right) + \frac{2\eta}{\gamma} C_m \frac{d\psi^*}{d\eta} = 0 \quad (14)$$

where

$$\eta = \frac{y}{2 \sqrt{\frac{k_m t}{a_m (b_m - 1) (\theta_{sm} - \theta_{rm}) \gamma}}} \quad , \quad \gamma = \frac{P_\infty^{b_m - 1}}{1 + P_\infty^{b_m - 1}} \quad , \quad P_\infty = -a_m \psi_\infty \quad (15)$$

The particular scales were chosen to minimize difficulties in numerical computations by taking advantage of the particular functional forms used for the matrix material curves. The seepage flux required in the solution of the fracture equation can be derived by using the similarity transformation in the definition given in (6). Given the rapid advance ratio, fracture to matrix, the lateral flux will be given, to a good approximation, by

$$v_w(x, t) = -\frac{1}{2} (P_\infty - P_0) \sqrt{\frac{k_m (b_m - 1) (\theta_{sm} - \theta_{rm}) \gamma}{a_m (t - t_0(x))}} \left. \frac{d\psi^*}{d\eta} \right|_{\eta=0} \quad (16)$$

where $t_0(x)$ represents the time for the moisture front to penetrate a distance x into the fracture; this function must be computed as part of the complete solution for the fracture. The seepage loss at x is defined only for $t > t_0$.

The nonlinear diffusion equation (14) governing the flow in the matrix was solved by a multi-parameter shooting technique developed by Griffiths,¹¹ which utilizes the Sandia National Laboratories SLATEC¹² mathematics library.

Flow in a Permeable-Walled Slot

If the fracture is idealized as a smooth permeable-walled slot with the effective material curves depicted in Figure 3, flow occurs only for pressure head greater than the value at the step transition; the relative permeability vanishes for pressure head below the step transition value. Denoting the location in the fracture where this value of pressure head

exists by $x = x(t)$ and neglecting the compressibility of water, the governing equations, (1) and (2), and boundary conditions describing the flow behind the front ($x \leq x(t)$) are given by

$$K_f \frac{\partial^2 h}{\partial x^2} + Q = 0$$

$$h = h_0 = \psi_0 \quad , \quad x = 0 \quad (17)$$

$$h = \psi_x - x(t) \quad , \quad x = x(t)$$

where ψ_x is the value of pressure head at $x(t)$ and $Q(x,t)$ is the loss term to the surrounding matrix.

Equation (17) can be integrated directly to give

$$h(x,t) - h_0 = (\psi_x - x - \psi_0) \frac{x}{x} - \frac{1}{K_f x} \left[x \int_0^x (x-\lambda) Q d\lambda - x \int_0^x (x-\lambda) Q d\lambda \right] \quad (18)$$

The location of the front $x(t)$ is determined by balancing the flux of material at the interface

$$\frac{dx}{dt} = -K_f \left. \frac{\partial h}{\partial x} \right|_{x=x} \quad (19)$$

resulting in

$$\frac{dx}{dt} + \frac{K_f}{x} (\psi_x - x - \psi_0) - \frac{1}{x} \int_0^x \lambda Q d\lambda = 0 \quad (20)$$

where $Q = -2V_w/w$ from equation (1). When the fracture is surrounded by an impermeable matrix, equation (20) is separable and has the solution

$$\tau = L - \log(1 + L) \quad (21)$$

where $L = x/\psi_c$, $\tau = K_f t/\psi_c$, and $\psi_c = \psi_0 - \psi_x$ is the capillary head driving the flow. With the exception of a sign change due to coordinate definitions, equation (21) is essentially the Washburn Equation¹³ describing the rise of a fluid in a capillary. Substituting the expression for the seepage loss, equation (16), equation (20) may be written as

$$\frac{dL}{d\tau} = 1 + \frac{1}{L} \left(1 - f \int_0^L \frac{\lambda d\lambda}{\sqrt{\tau - \tau_0(\lambda)}} \right) \quad (22)$$

where f is a dimensionless seepage loss parameter given by

$$f = -(P_\infty - P_0) \sqrt{\frac{k_{sm}}{k_{sf}} \left(\frac{\psi_c}{w}\right)^2 \left(\frac{1}{a_m \psi_c}\right) (b_m - 1) (\theta_{sm} - \theta_{rm}) \gamma} \left. \frac{\partial \psi^*}{\partial \eta} \right|_{\eta=0} \quad (23)$$

and $\tau_0(L)$ is the time required for the moisture front to penetrate a distance L , i.e., the inverse of the desired solution $L(\tau)$. The solution of equation (22) provides the moisture penetration history in a permeable-walled slot and the necessary data to compute hydraulic head profiles from equation (18). Fluxes in the fracture are given by differentiation of equation (18):

$$-K_f \frac{\partial h}{\partial x} = K_f \left(\frac{\psi_0 - \psi_x}{x} \right) + K_f + \frac{1}{x} \left[\int_0^x x Q d\lambda - \int_0^x (x - \lambda) Q d\lambda \right] \quad (24)$$

Equation (22) was solved with the ordinary differential equation (ODE) and numerical integration routines available in the Sandia SLATEC¹² mathematics library.

Flow in a Sandy Fracture

Natural fractures have some pore structure and roughness⁴ associated with them and are far from smooth. The pore structure will also depend on the effective stress.¹⁴ Although the capillary characteristics have not, as far as we are aware, been measured, the pore structure should have some of the characteristics mentioned previously. We assume that natural fracture material characteristics may be adequately described by the general van Genuchten and Mualem functions used to fit material data for the matrix. Material properties characteristic of sand or soil can be fit to the functions. This is equivalent to simulating the natural fracture as a high-permeability layer filled with the soil material.

Nondimensionalization of the fracture equation reveals the form of the loss parameter from fracture to matrix. Introducing the following normalized variables

$$H = \frac{\psi - \psi_{\infty}}{\psi_0 - \psi_{\infty}}, \quad x^+ = xa_f, \quad t^+ = \frac{a_f K_f t}{(b_f - 1)(\theta_{sf} - \theta_{rf})} \quad (25)$$

$$\Delta P = a_f(\psi_0 - \psi_{\infty}), \quad C_f(P(H)) = \frac{P^{b_f-1}}{(1 + P^{b_f})^{c_f+1}}, \quad c_f = 1 - 1/b_f,$$

equations (1) and (2) combine to give

$$C_f(H) \frac{\partial H}{\partial t^+} = \frac{\partial}{\partial x^+} \left[k_{rf} \left(\frac{\partial H}{\partial x^+} + \frac{1}{\Delta P} \right) \right] - \sqrt{\frac{q}{(t^+ - t_0^+)}} \frac{\partial \psi^*}{\partial \eta} \Big|_{\eta=0} \quad (26)$$

As for the smooth slot, $t_0^+(x^+)$ is the time for the "moisture front" to reach x^+ . Here the front is defined as some characteristic moisture content greater than the initial value $\theta_f(\psi_{\infty})$. The loss parameter, q , is given by

$$q = \frac{k_{sm}}{k_{sf}} \frac{1}{(wa_f)^2} \frac{a_m (b_m - 1)}{a_f (b_f - 1)} \left(\frac{\theta_{sm} - \theta_{rm}}{\theta_{sf} - \theta_{rf}} \right) \gamma \quad (27)$$

and also depends on ratios of matrix to fracture permeability and length scales for the problem.

The governing equation was solved in dimensional form, equations (1) and (2), by a method of lines technique.⁵ The set of ODEs resulting from applying finite differences to the spatial terms is shown in Appendix A. The Sandia SLATEC¹² math library routine DEBDF, designed for mildly stiff equations, was used to integrate the resulting set of ODEs in time.

APPLICATION TO YUCCA MOUNTAIN

Material Properties for Yucca Mountain

Material properties for the Yucca Mountain region of the Nevada Test Site have been determined from laboratory measurements performed on core samples from various geologic units. The measurements were performed by Pacific Northwest Laboratory (PNL) and the data reduced into a suitable format by members of the NNWSI Repository Performance Assessment Division at Sandia Laboratories.¹⁵ The data was fit to the van Genuchten and Mualem functions presented previously. The parameter values used in this study for the hydrologic units at Yucca Mountain are listed in Table 1 and are approximately the same as the final data fits presented by Peters, et al.¹⁵ Figures 4 through 7 show the saturation (θ_m/θ_{sm}) and relative permeability curves as functions of suction head. Suction head is the negative of the pressure head used in this report.

Flow in Yucca Mountain Materials

Solutions for the one-dimensional flow in the matrix region due to an abrupt jump to saturation at the fracture plane ($y = w/2$ in Figure 1) were computed for all geologic units in Table 1 except for the Calico Hills nonwelded (zeolitized) unit because of its similarity to the Topopah Spring unit. The major difference between the materials is the porosity, θ_{sm} , which appears only as a scale parameter in the nondimensionalization. Solution results for the Calico Hills nonwelded (zeolitized) unit can be inferred from those of the Topopah Spring with a rescaling of parameters involving the porosity. The similarity solutions provide the necessary data to compute the lateral seepage parameters for the smooth and sandy fracture models. Solutions for initial saturations of 90%, 75%, 50%, and 25% are shown in Figures 8 through 11 in the normalized variables. These figures provide complete solutions of horizontal one-dimensional capillary conduction of moisture for material units representative of Yucca Mountain.

Although the equations were scaled to lessen the effects of the nonlinear material properties, the nonlinearities are still evident in the solutions. The solutions become steeper with decreasing initial saturation and approach a front-like solution as the initial saturation tends to the residual moisture content. This behavior is familiar to those simulating moisture absorption by desiccated soils¹⁶ and is a source of numerical difficulty because of the sharp front.

Table 1. Matrix Properties for Yucca Mountain

Geological Unit	Sample Code	θ_{sm}	$\theta_{rm}/\theta_{sm}^*$	a_m^* (cm^{-1})	b_m^*	K_m (cm/s)
Calico Hills nonwelded (vitric)	GU3-14	0.42	0.0747	0.890E-4	5.862	2.7E-05
Calico Hills nonwelded (zeolitized)	G4-11	0.33	0.0809	0.365E-4	1.489	2.0E-09
Topopah Spring welded (Rep. and Litho. Zone)	G4-6	0.094	0.0669	0.519E-4	1.787	1.9E-09
Paintbrush nonwelded	GU3-7	0.41	0.1178	0.151E-3	6.966	3.9E-05
Tiva Canyon welded	G4-1	0.070	0.0400	0.144E-3	1.470	1.3E-09

*These parameter values are approximately the same as the final fits from saturation data presented by Peters, et al.¹⁵

The source term for the fracture equations can be obtained from the similarity solutions through the use of equation (16). Table 2 lists values of the inlet boundary gradient computed in the similarity solutions. These values provide the necessary data for computing the moisture penetration history in the fracture.

Flow in the Fracture

The penetration distance of moisture into the fracture is of primary importance in assessing the significance of the presence of fractures on transporting infiltration. The variation of penetration with time for the smooth slot, equation (22), is illustrated in Figure 12 for various values of the loss parameter. The figure shows that the penetration can be substantially mitigated even for loss parameters of order unity. The relative

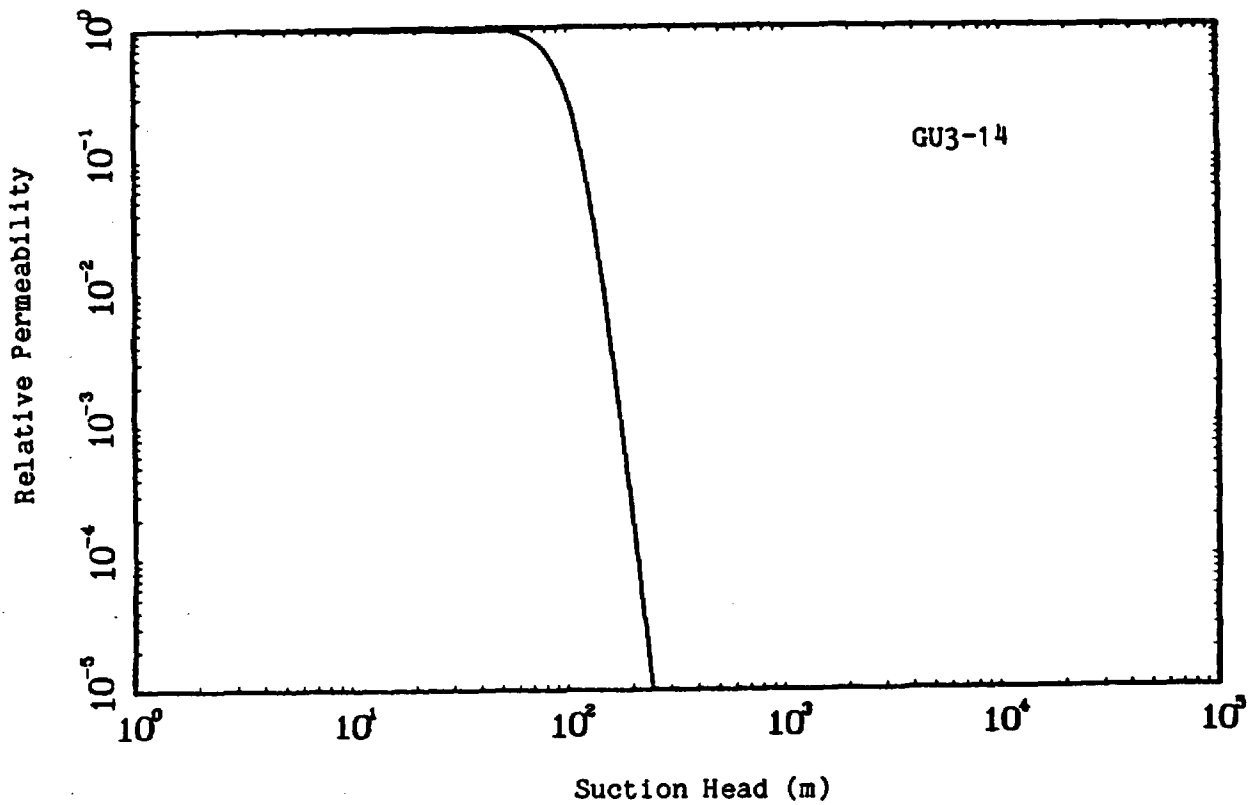
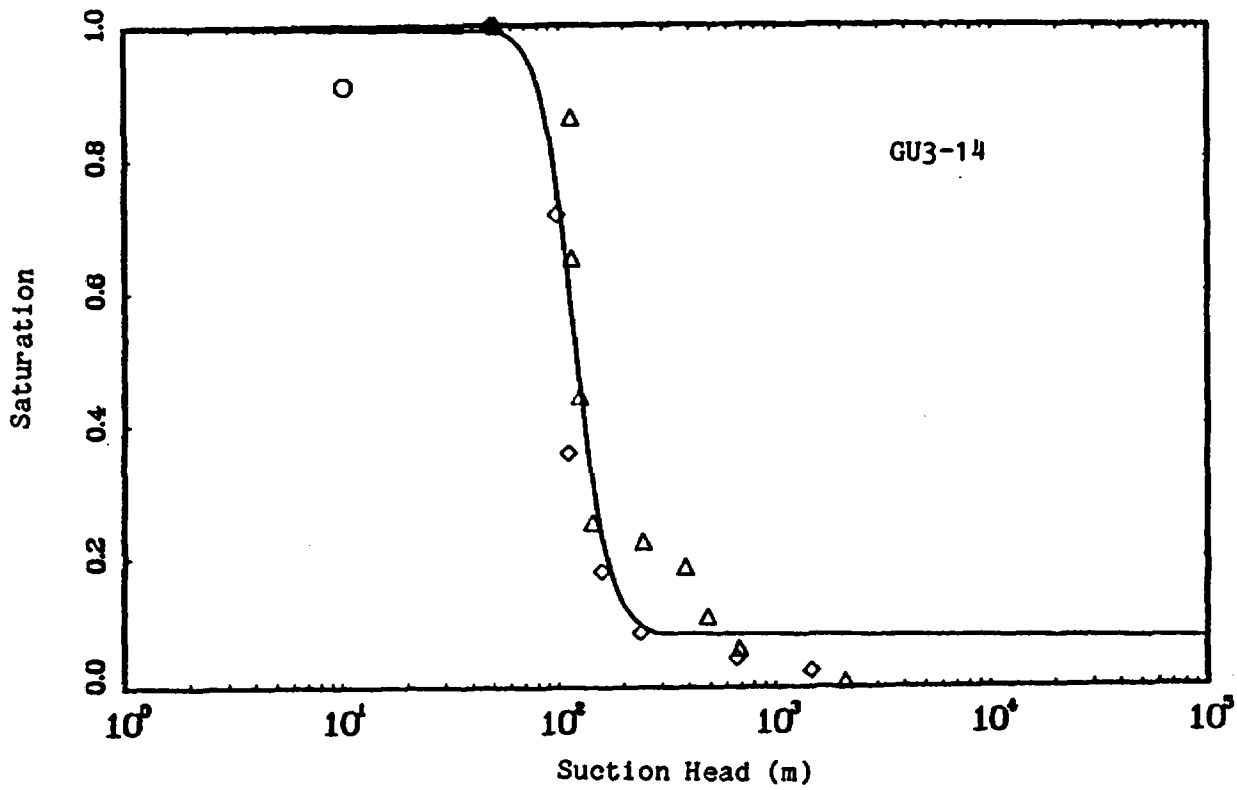


Figure 4. Material properties for the Calico Hills nonwelded vitric unit; symbols denote data and curves the material model representation (after Peters, et al.¹⁵).

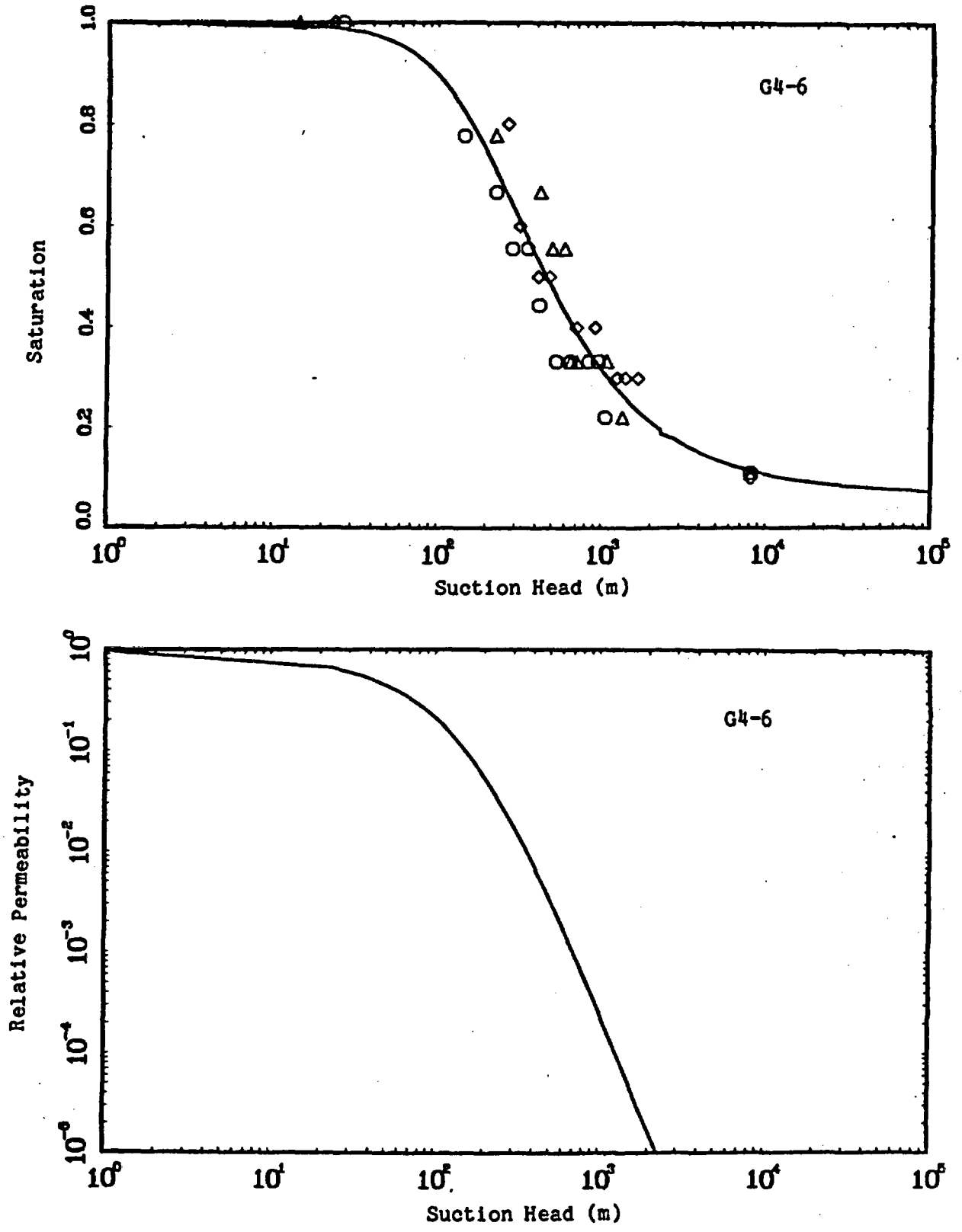


Figure 5. Material properties for the Topopah Spring welded unit; symbols denote data and curves the material model representation (after Peters, et al. 19).

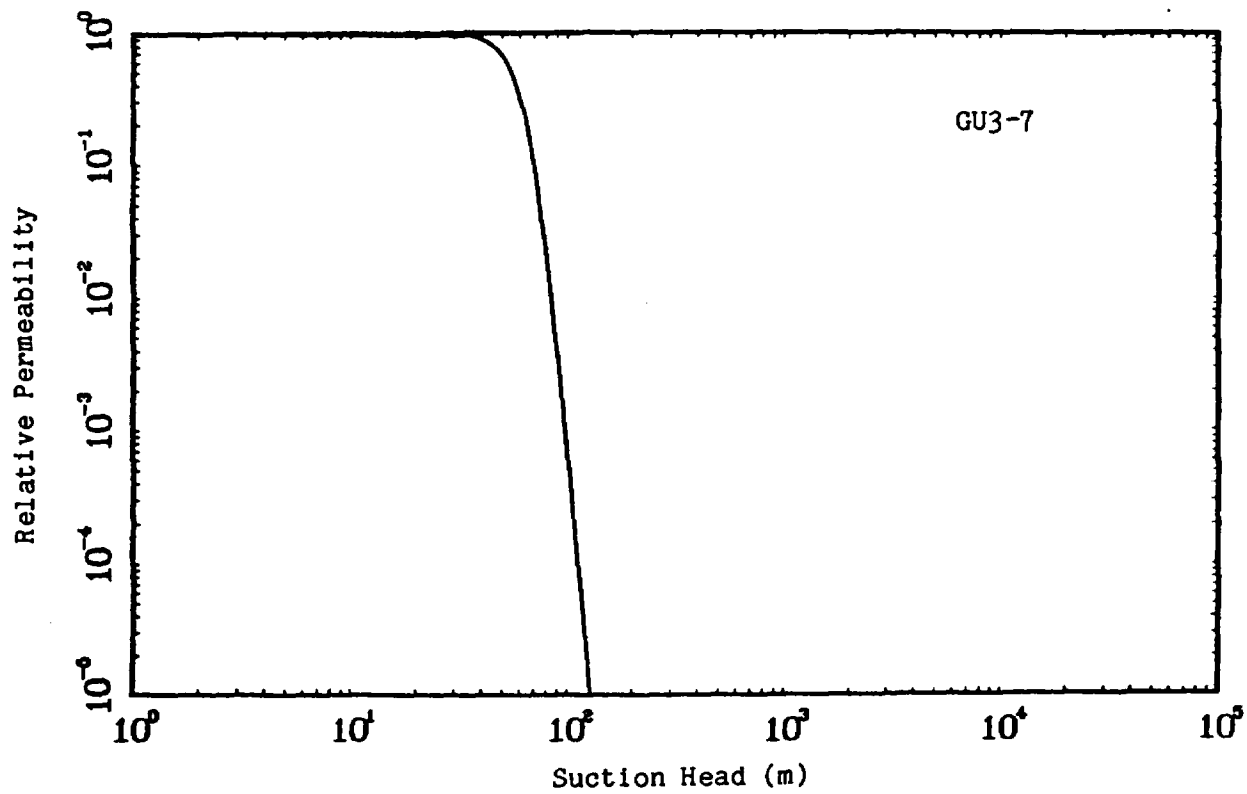
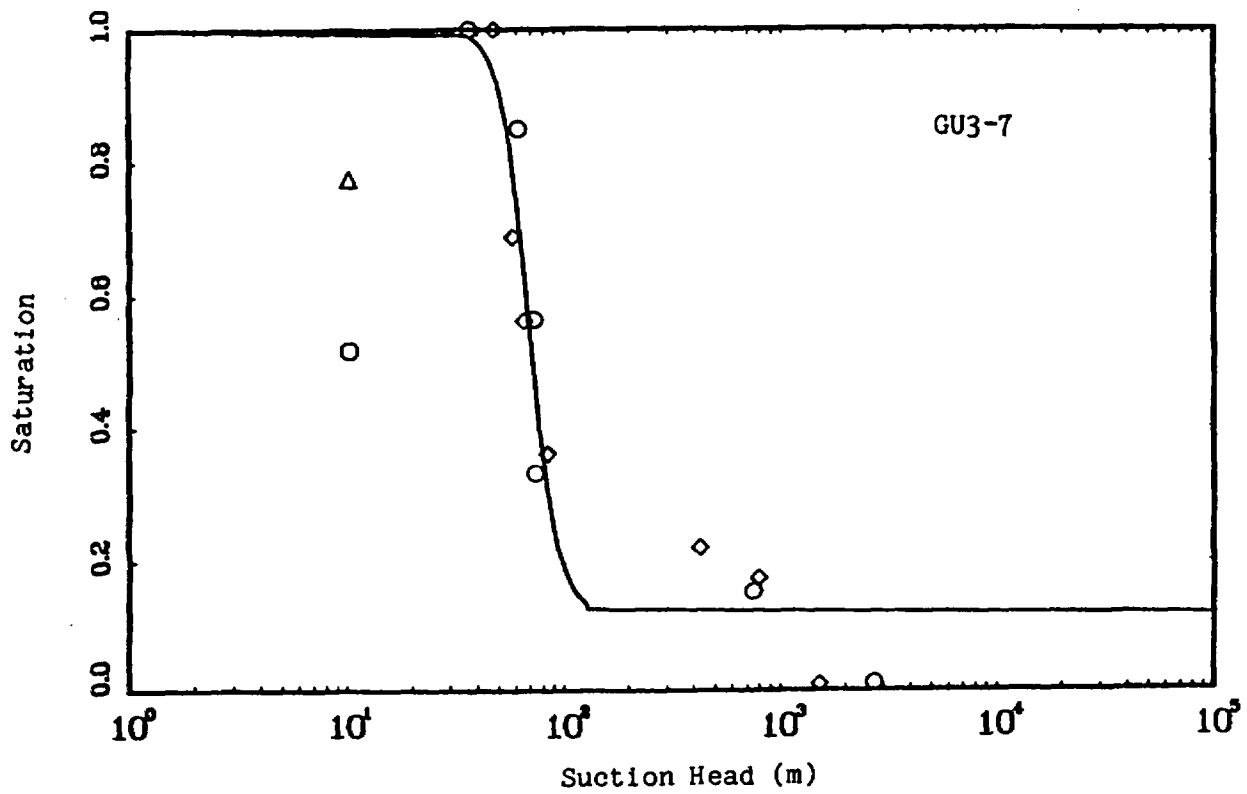


Figure 6. Material properties for the Paintbrush nonwelded unit; symbols denote data and curves the material model representation (after Peters, et al.¹⁵).

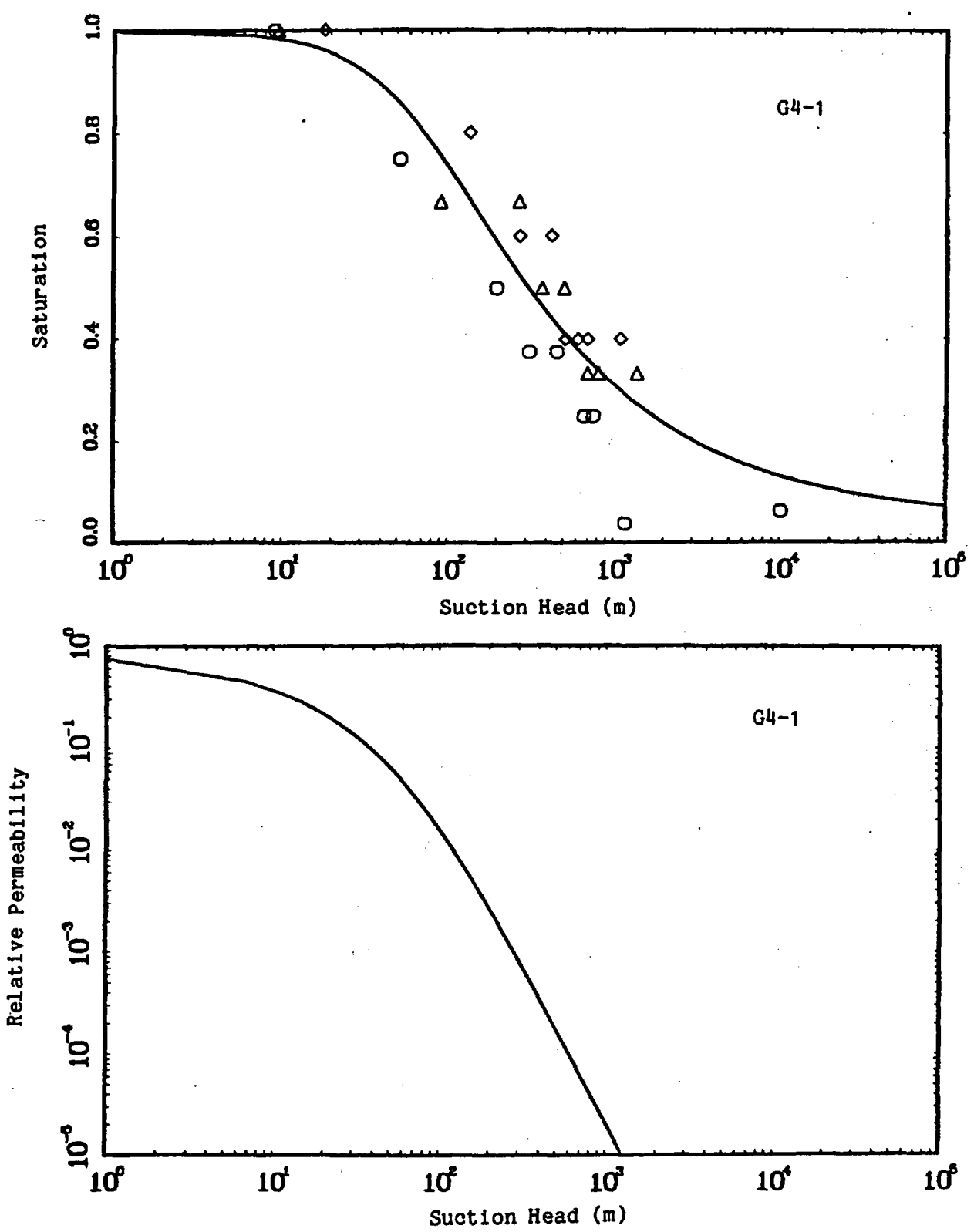


Figure 7. Material properties for the Tiva Canyon welded unit; symbols denote data and curves the material model representation (after Peters, et al. 15).

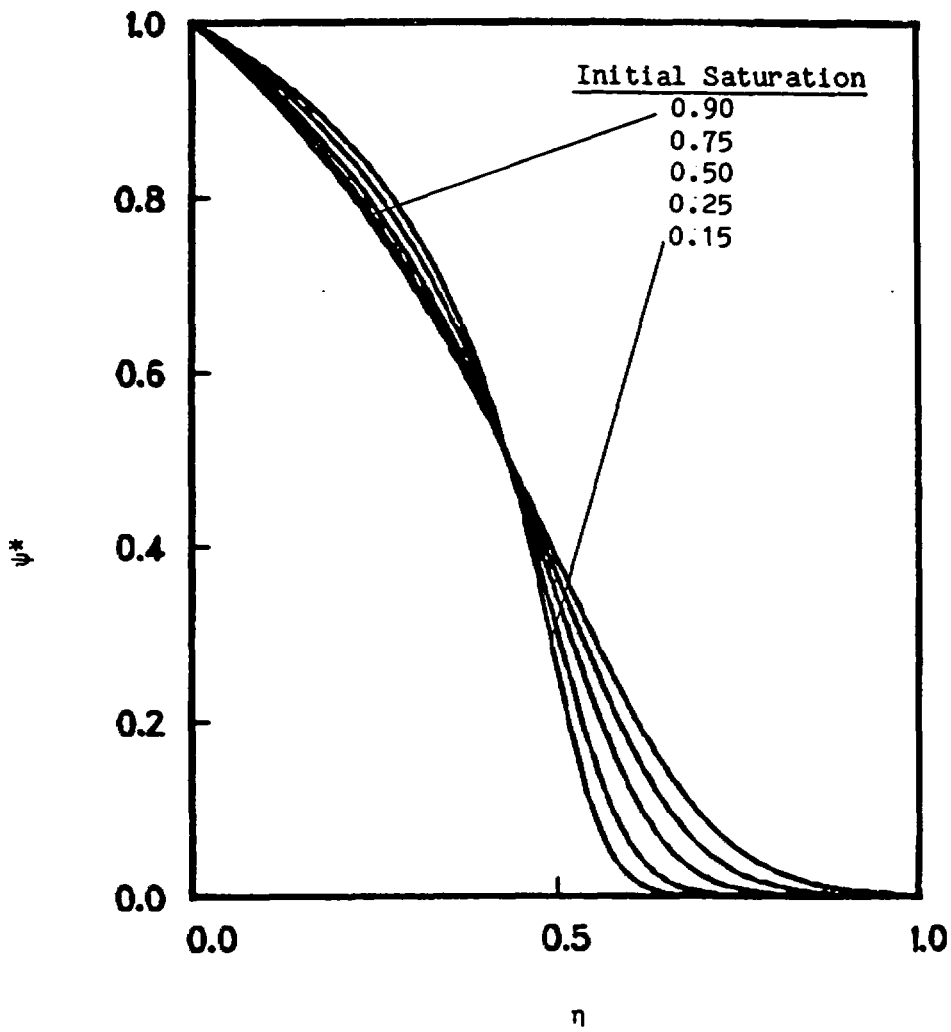


Figure 8. Pressure head distribution in the Calico Hills nonwelded (vitrific) unit.

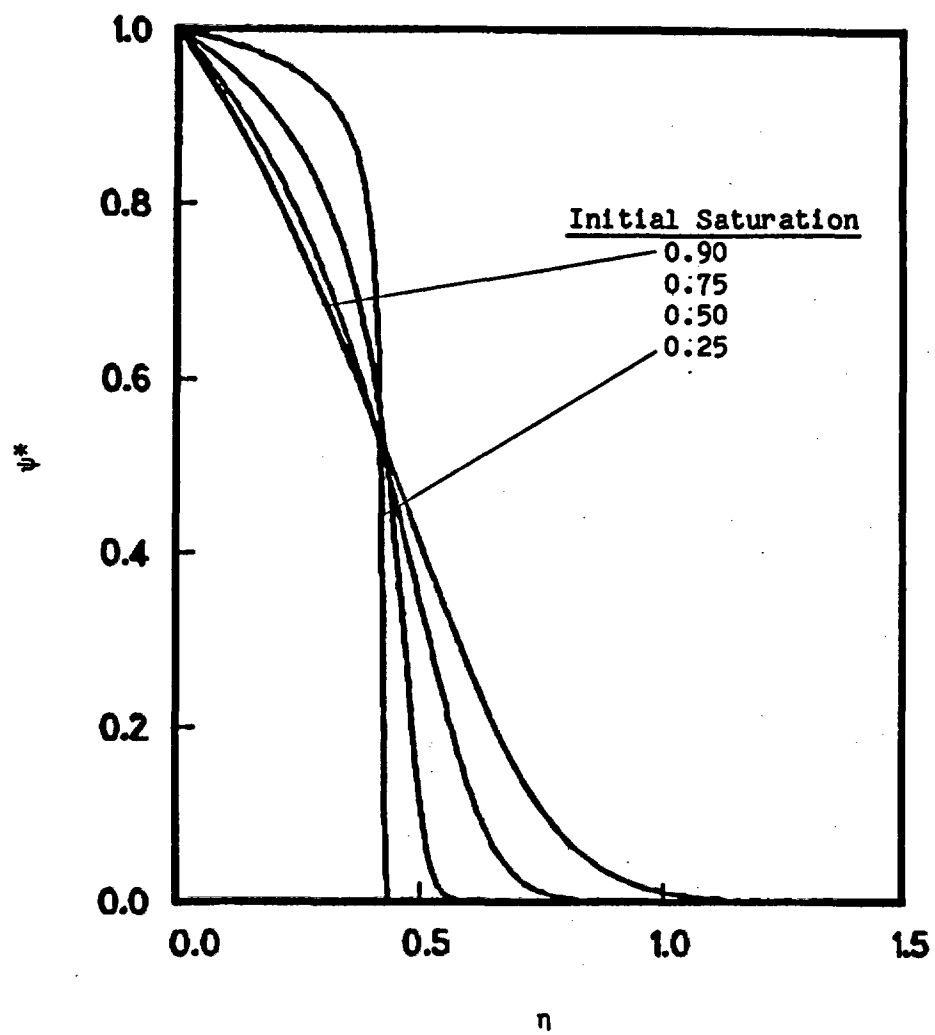


Figure 9. Pressure head distribution in the Topopah Spring welded unit.

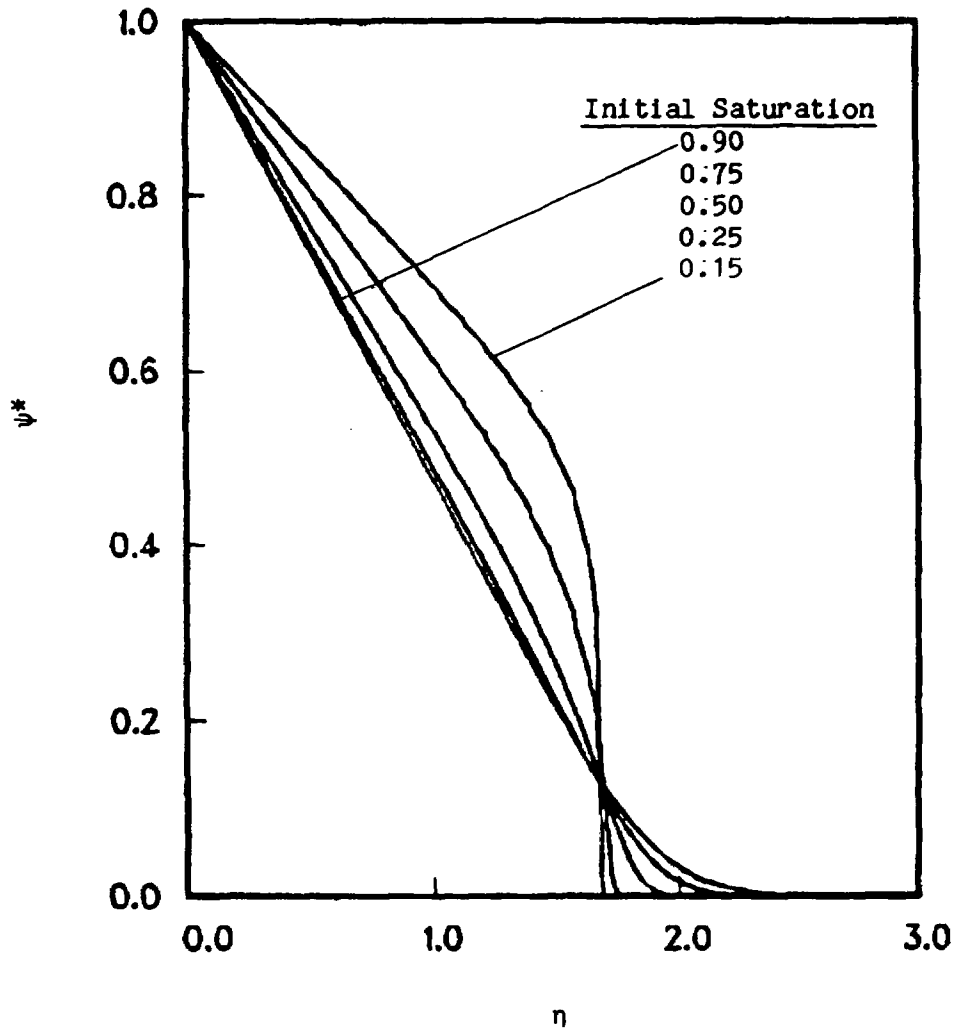


Figure 10. Pressure head distribution in the Paintbrush nonwelded unit.

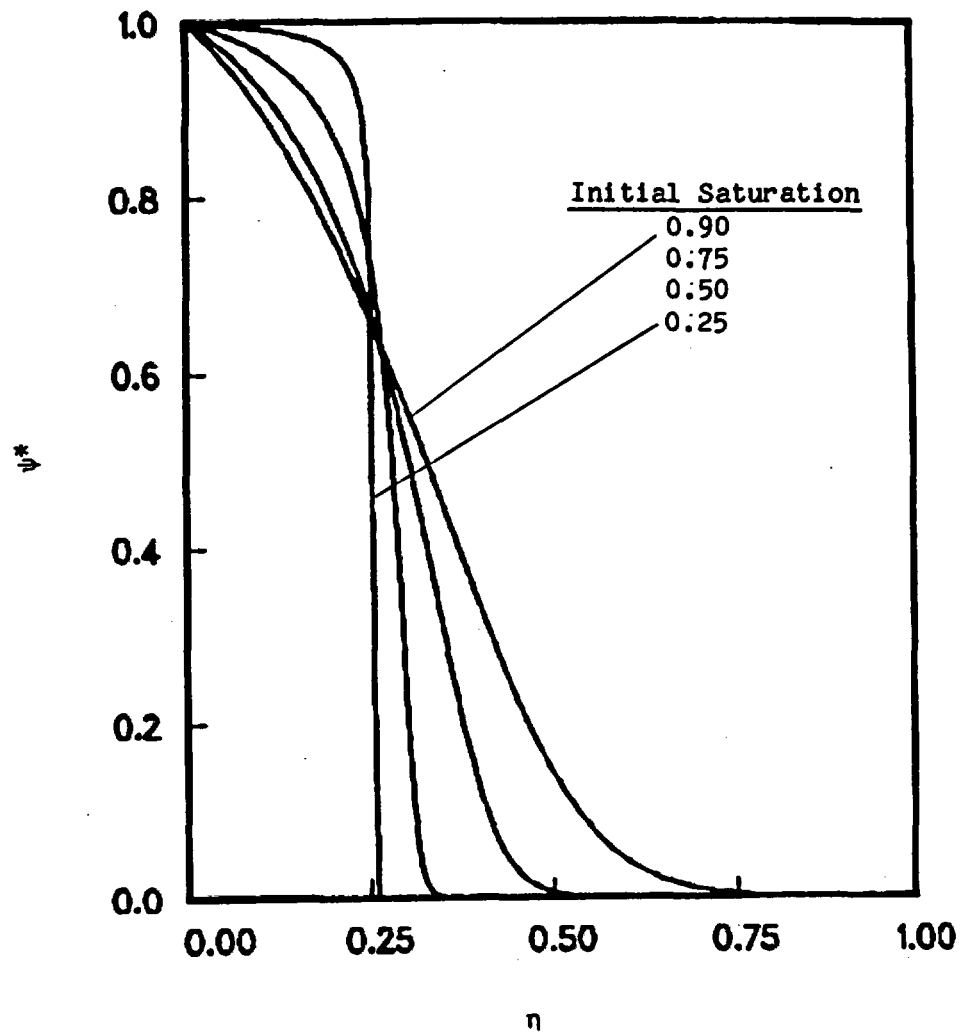


Figure 11. Pressure head distribution in the Tiva Canyon welded unit.

Table 2. Boundary Gradient ($\frac{d\psi^*}{d\eta}\bigg|_{\eta=0}$) from Matrix Flow Solutions

Unit	Initial Saturation			
	90%	75%	50%	25%
Calico Hills nonwelded (vitric)	-0.705	-0.650	-0.585	-0.506
Topopah Spring welded	-0.791	-0.604	-0.337	-0.114
Paintbrush nonwelded	-0.525	-0.510	-0.467	-0.385
Tiva Canyon welded	-0.685	-0.446	-0.184	-0.037

moisture penetration for different materials and various initial matrix saturations can be inferred from values of the loss parameter arising in the smooth slot equation. Loss parameters, as defined in equation (23), for all matrix materials and initial saturations computed for the similarity solutions are listed in Tables 3-6. The values indicate the Topopah Spring and Tiva Canyon units will allow the most fracture penetration for large fracture apertures and high initial saturations.

The limit of an impermeable matrix offers a "worst case" for moisture transport in a fractured material caused by episodic infiltration. The smooth slot equation can be integrated directly for this case, and the solution is given in (21) in terms of normalized variables. The capillary driving force, ψ_c , provides the length scale in this case and may be computed from the capillary rise equation for a slot presented in equation (7). The one-dimensional infiltration equation governs the transport in the sandy fracture for the impermeable matrix limit. The particular capillary curve chosen to model the sandy fracture is that used by Freeze¹⁷ in his

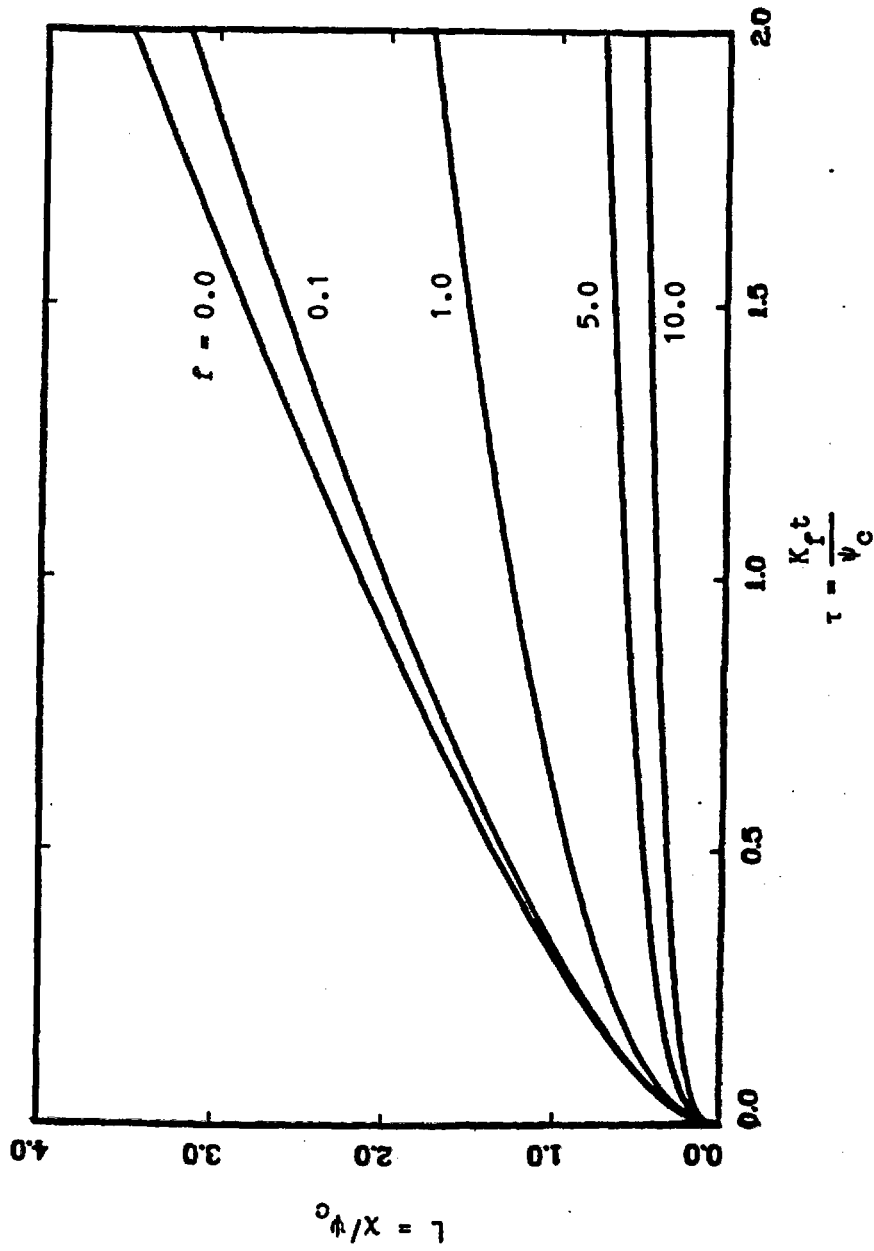


Figure 12. Variation of fracture moisture penetration with loss parameter f .

numerical analysis of vertical infiltration. The fit parameters were determined by Klavetter and Peters¹⁸ to be

$$a_f = 1.285 \text{ m}^{-1}$$

$$b_f = 4.229$$

$$\theta_{rf} = 3.95 \times 10^{-2}$$

Table 3. Loss Parameters, f , for Smooth Slot (Eqn. (23)) Fracture Model for Calico Hills Nonwelded

Aperture (μm)	Initial Saturation			
	90%	75%	50%	25%
100	120	192	278	362
75	214	342	405	645
50	482	770	1110	1450
25	1930	3080	4460	5800

Table 4. Loss Parameters, f , for Smooth Slot (Eqn. (23)) Fracture Model for Topopah Spring

Aperture (μm)	Initial Saturation			
	90%	75%	50%	25%
100	0.29	0.53	0.79	0.98
75	0.52	0.93	1.40	1.74
50	1.17	2.10	3.15	3.92
25	4.66	8.41	12.6	15.7

Table 5. Loss Parameters, f , for Smooth Slot (Eqn. (23)) Fracture Model for Paintbrush

Aperture (μm)	Initial Saturation			
	90%	75%	50%	25%
100	92.1	153	221	273
75	163	272	394	486
50	368	611	886	1090
25	1470	2440	3550	4370

Table 6. Loss Parameters, f , for Smooth Slot (Eqn. (23)) Fracture Model for Tiva Canyon

Aperture (μm)	Initial Saturation			
	90%	75%	50%	25%
100	0.10	0.18	0.27	0.34
75	0.18	0.32	0.48	0.61
50	0.40	0.72	1.08	1.38
25	1.59	2.88	4.34	5.51

for use in the van Genuchten and Mualem functions. The fracture porosity was set to unity for the calculations. The particular capillary curve chosen to model the sandy fracture represents the assumed pore structure (recall the discussion of material models) and, hence, some characteristic macroscopic capillary force. It is found that a capillary driving head, ψ_c , of 60 cm provides a good comparison between solutions for penetration histories from both fracture models. The location of the front for the sandy fracture model was defined as 50% saturation. The comparison is shown in Figure 13 by the curve labeled $f = 0$. From the capillary rise

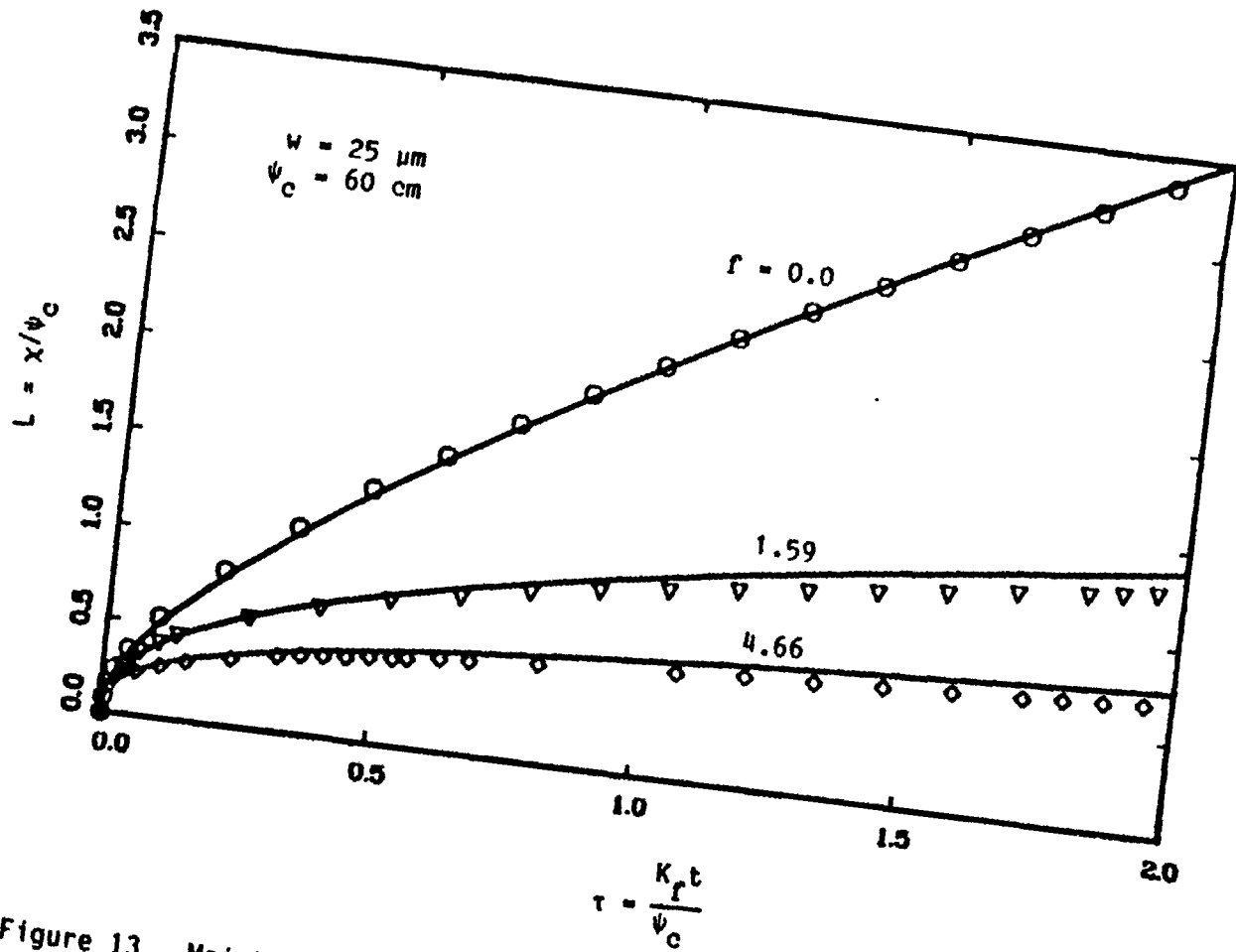


Figure 13. Moisture penetration for a 25 μm fracture located in an impermeable matrix ($f=0$), the Tiva Canyon (1.59) and the Topopah Spring (4.66). The smooth slot (curves) and sandy fracture (symbols) models give comparable penetrations.

equation (7), the 60 cm capillary head implies a 25 μm aperture for $\alpha = 0$. Thus, the capillary curve chosen for the sandy fracture is representative of a 25 μm smooth slot. Figures 14 and 15 show profiles of pressure head, moisture content, conductivity, and Darcy flux along the fracture at selected times, as given by the numerical solution for the sandy fracture. The pressure head profiles are typical of an invading moisture pulse in the fracture. The linear portion of the pressure head profile is a region of high saturation and consequently large conductivity; the flux is nearly constant in this region. The front is a consequence of rapidly varying capillary and permeability curves and the low initial saturation for the fracture (residual saturation for the fill material). The solution is indicative of a quasi-steady flow in which viscous forces balance pressure gradients and the position of the front is determined by the necessity to balance the mass flux. These are the assumptions for the smooth slot approximation.

Having determined the representative capillary driving force embodied in the capillary curve for the sandy fracture, we may proceed to compare solutions for a permeable matrix using a value $\psi_c = 60$ cm in the smooth slot equations. From Tables 4 and 6, we find the Topopah Spring and Tiva Canyon members provide the worst case materials for fracture flow in a 25 μm fracture. Figure 13 shows fracture moisture penetration histories as given by the smooth slot and sandy fracture models for the loss parameters from Tables 4 and 6. The solutions were computed to a normalized time of 2, representing approximately 30 minutes of physical time for a 25 μm aperture. The significance of the seepage loss to the matrix is illustrated by the mitigation of moisture penetration even for small loss coefficients. The extreme case of an impermeable matrix indicates a penetration of approximately 2 m over 30 minutes of infiltration.

Figures 16 through 19 show profiles of pressure head, moisture content, conductivity, and Darcy flux along the fracture for selected times, as given by the numerical solution for the sandy fracture in both the Topopah Spring and Tiva Canyon units. The pressure head profiles again exhibit a linear portion from inlet to the position of the front. The flux profiles, on the other hand, now decrease nearly linearly from inlet to moisture front departing from the nearly constant solutions given when the matrix is impermeable.

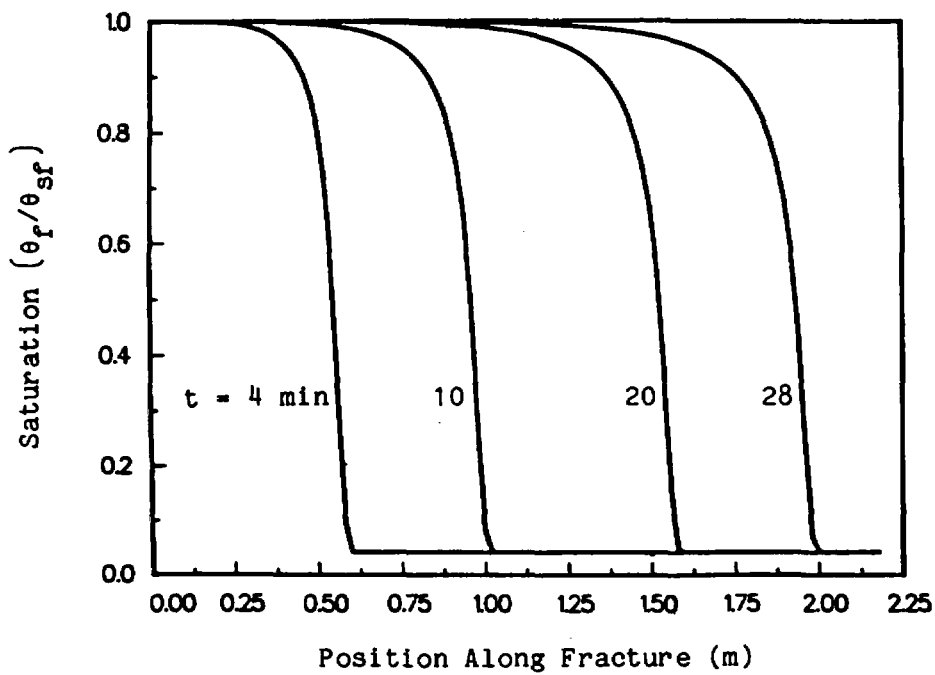
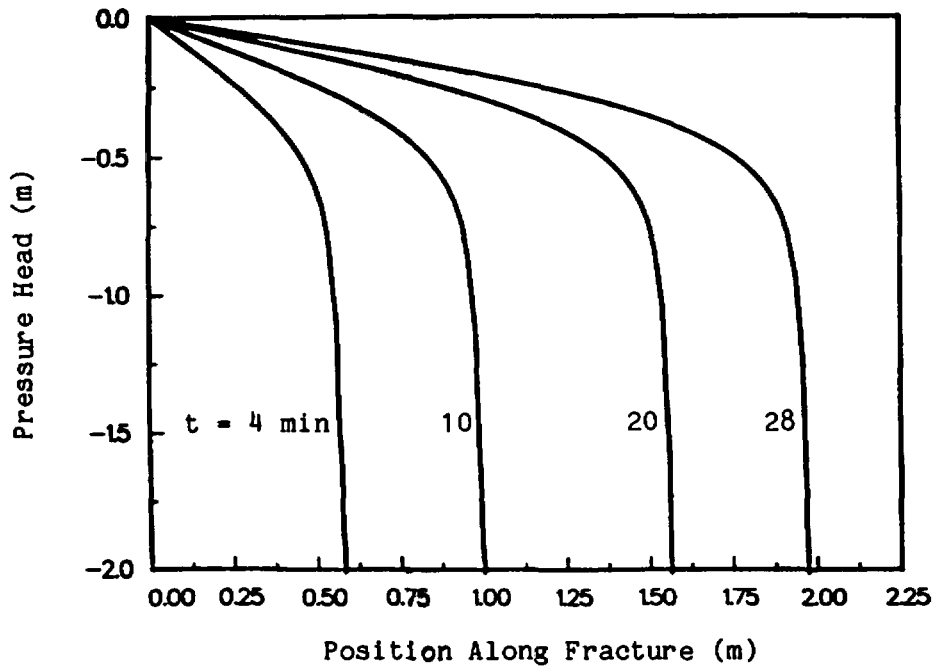


Figure 14. Pressure head and saturation distributions in a 25 μm fracture embedded in an impermeable matrix.

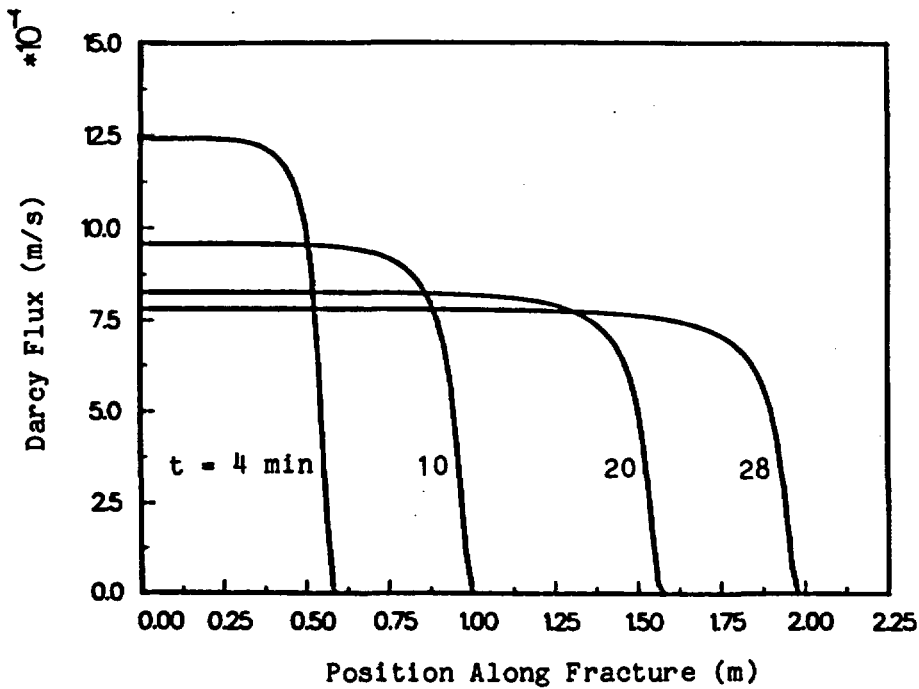
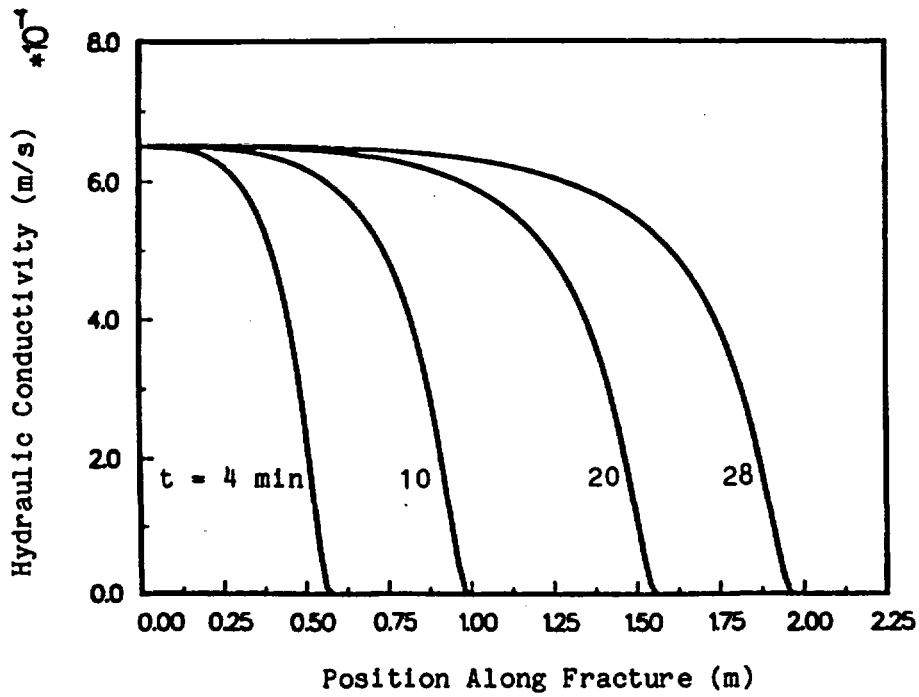


Figure 15. Hydraulic conductivity and Darcy flux distributions in a 25 μm fracture embedded in an impermeable matrix.

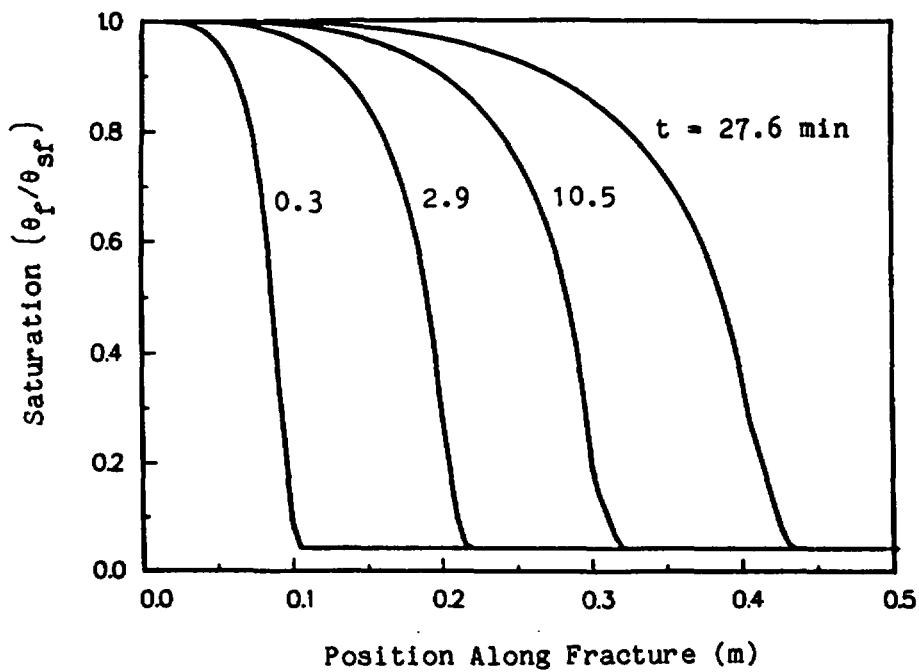
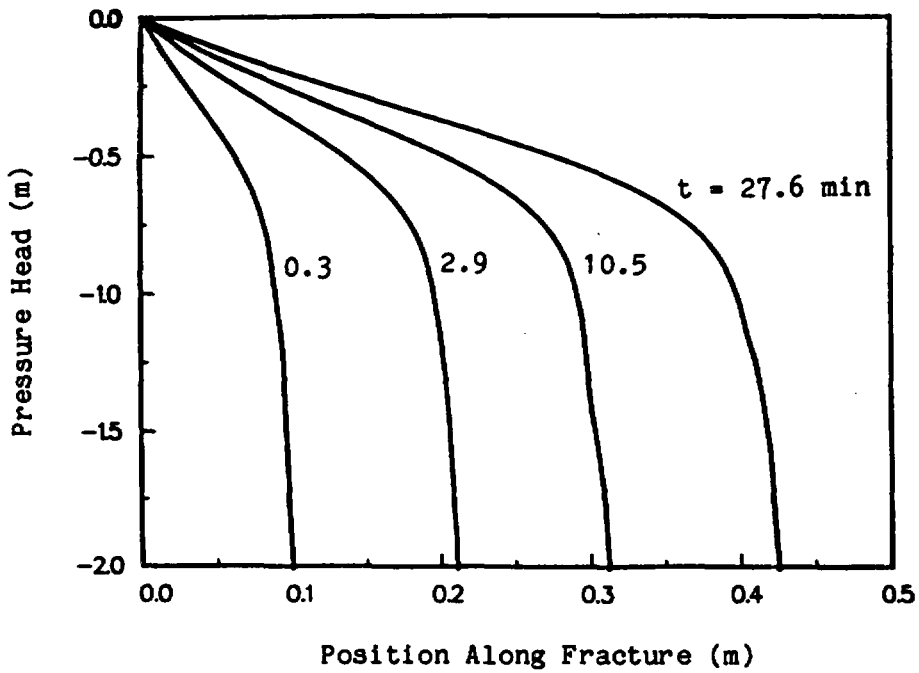


Figure 16. Pressure head and saturation distributions in a $25 \mu\text{m}$ fracture located in the Topopah Spring welded unit.

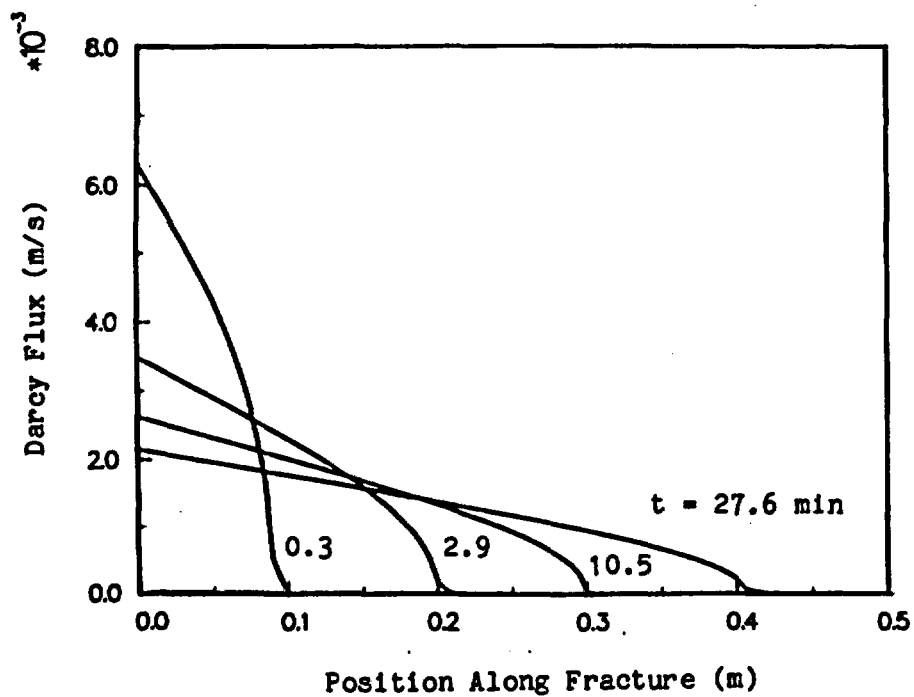
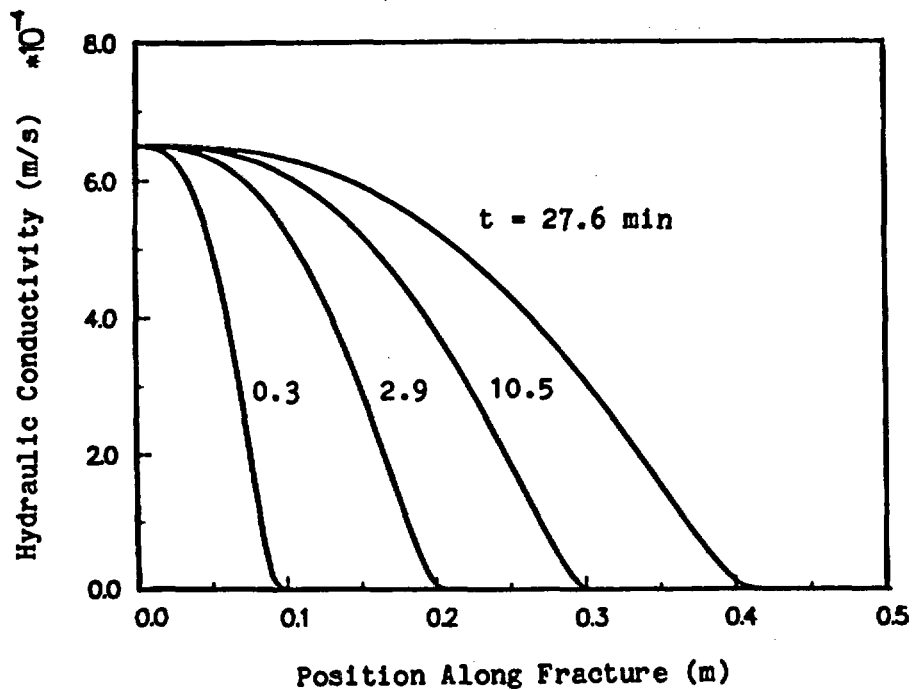


Figure 17. Hydraulic conductivity and saturation distributions in a 25 μm fracture located in the Topopah Spring welded unit.

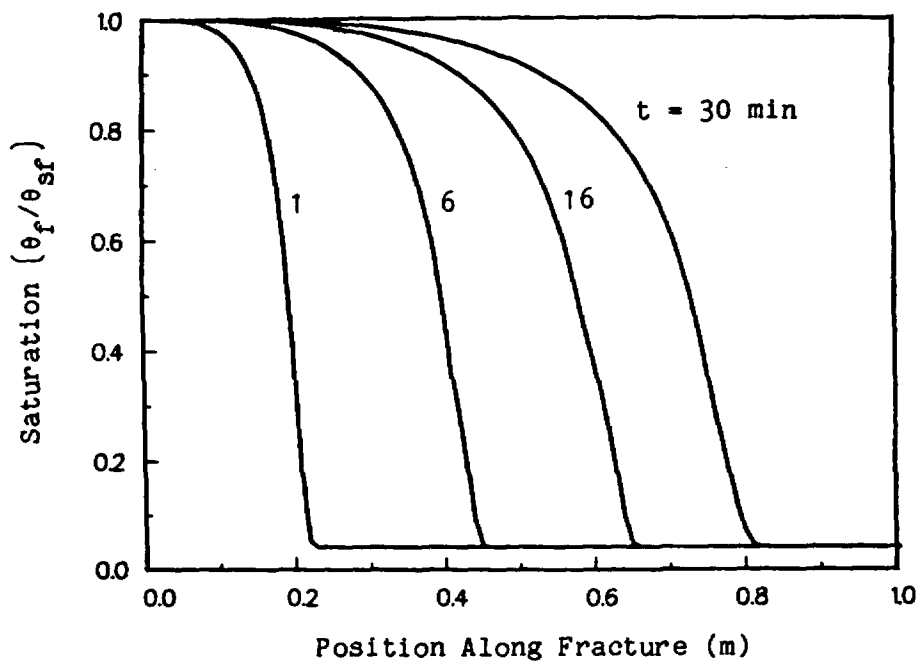
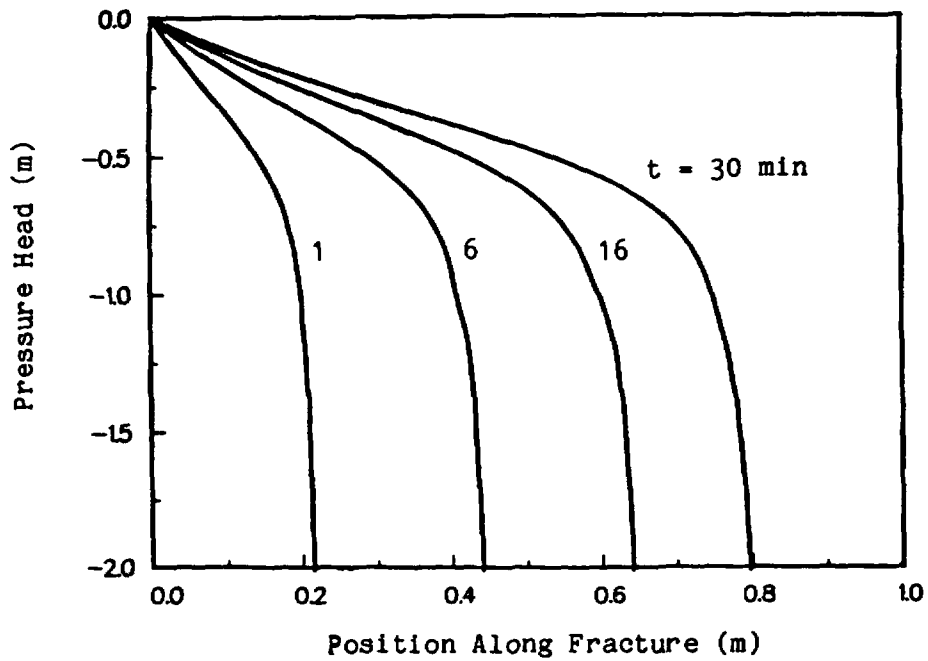


Figure 18. Pressure head and saturation distributions in a 25 μm fracture located in the Tiva Canyon welded unit.

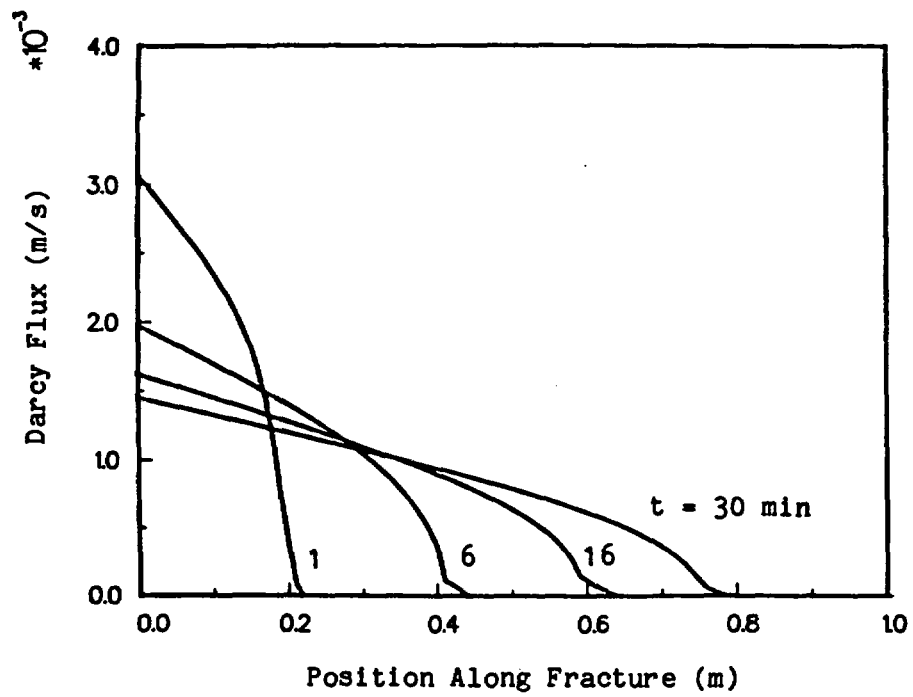
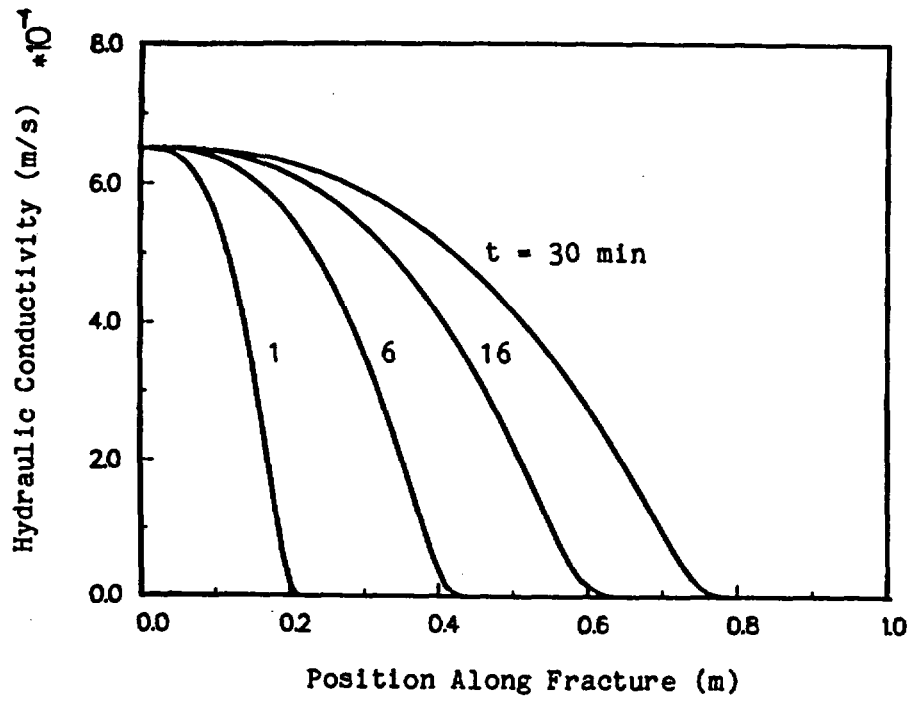


Figure 19. Hydraulic conductivity and Darcy flux distributions in a 25 μm fracture located in the Tiva Canyon welded unit.

Additional solutions for penetration histories were computed for a 100 μm smooth slot and are shown in Figure 20. The 100 μm fracture should provide a nominal upper bound on natural fracture apertures. Peters et al.¹⁵ suggest values of 15 μm or less. The values of seepage loss parameters correspond to values for the Topopah Spring and Tiva Canyon units in Tables 4 and 6. The computation was carried out to 30 minutes as before. The capillary driving head for this case is 15 cm, computed from equation (7) for $\cos\alpha = 1$. The figure shows penetrations of 19.5, 9.8, and 4.9 m for seepage loss parameters of 0, 0.10, 0.29, respectively, after 30 minutes of infiltration.

Solutions for fracture moisture penetrations given in Figures 12, 13, and 20 are actually general rather than applying only to a particular aperture. The figures show solutions to equation (22) describing flow in a permeable-walled smooth slot for loss parameters in Tables 4 and 6. The capillary parameter, ψ_c , does not appear explicitly in equation (22) but is required for interpretation of the solution. Since ψ_c depends on the aperture according to equation (7), the solutions can represent any fracture aperture. Having determined ψ_c from (7), the moisture penetration and time in physical units are given by

$$x = L\psi_c \quad , \quad t = \tau\psi_c/K_f$$

for values of $L(\tau)$ given in Figures 12, 13, and 20. The loss parameter is determined from equation (23), which depends on the aperture among other problem parameters.

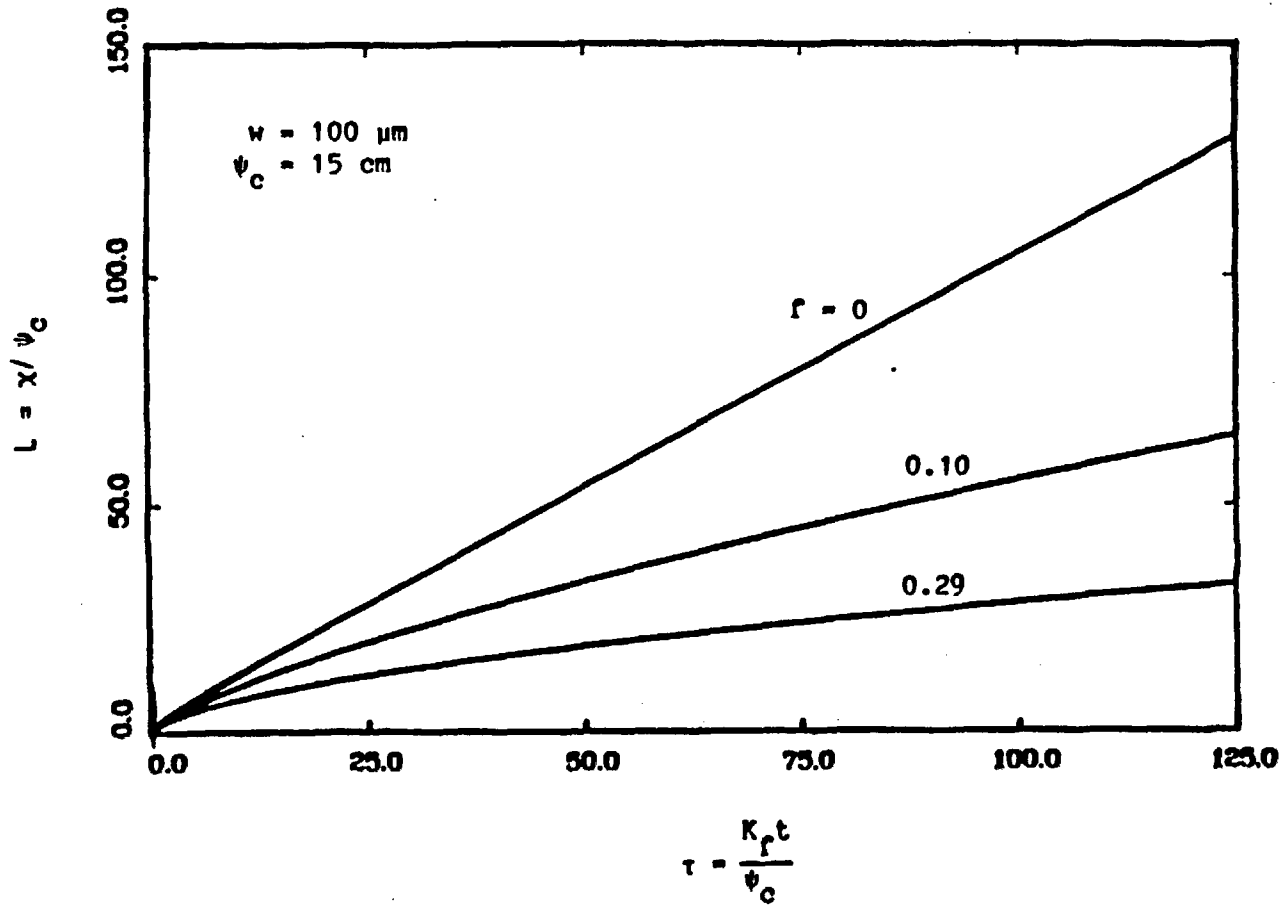


Figure 20. Moisture penetration for a 100 μm fracture as given by the smooth slot model. The matrix material is impermeable ($f=0$), the Tiva Canyon (0.10), and the Topopah Spring (0.29).

SUMMARY

Capillary-driven flow along an isolated fracture located in a porous material can be modeled by idealizing the fracture as a smooth slot or a high-permeability slot filled with a coarse material. Flow is induced in the fracture by imposing full saturation at the inlet. Because of the large contrast between the fracture and matrix material properties, the initial saturation in the fracture is the residual saturation for the fill material (complete desiccation for the smooth slot model). The models predict parameters of engineering interest such as moisture penetration, Darcy flux along the fracture, and the dependence of fracture to matrix seepage losses on material parameters and length scales in the problem. In particular, the penetration is shown to be a strong function of the seepage loss parameter, which depends on matrix-fracture permeability and length scale ratios.

The models were applied to materials representative of the Yucca Mountain region of the Nevada Test Site, a potential nuclear waste repository site. Loss parameters were found to be large, indicating small moisture penetrations along the fracture, for most geologic units. The calculations were computed for a 30 minute infiltration period, which was assumed as a nominal upper bound for precipitation events in arid regions. Results based on a 25 μm fracture indicate fracture moisture penetrations of approximately 40 and 80 cm for the Topopah Spring and Tiva Canyon units during a 30 minute infiltration event. Because of their low loss parameters, the Topopah Spring and Tiva Canyon units offer the most potential for significant fracture transport of moisture, seepage loss parameters for the remaining geologic units being large. Calculations based on a 100 μm fracture for the smooth slot model indicate penetrations of 4.9 and 9.8 m for the Topopah Spring and Tiva Canyon, respectively. The data reported by Peters, et al.¹⁵ indicate apertures of 15 μm or less. The models would predict small penetrations for this range of aperture. However, penetrations increase dramatically with increasing fracture aperture.

REFERENCES

- (1) G. I. Barenblatt, Iu. P. Zheltov, and I. N. Kochina, "Basic Concepts of the Theory of Seepage of Homogeneous Liquids in Fissured Rock," P.M.M., 24, No. 5, 1960, 852-864.
- (2) J. E. Warren and P. J. Root, "The Behavior of Naturally Fractured Reservoirs," Soc., Pet. Eng. J., Vol. 3, Sept. 1963, 245-255.
- (3) D. T. Snow, "A Parallel Plate Model of Fractured Permeable Media," Ph.D. Thesis, University of California, Berkeley, CA, 1965.
- (4) K. Iwai, "Fundamental Studies of Fluid Flow Through a Single Fracture," Ph.D. Thesis, Department of Civil Engineering, University of California, Berkeley, CA, 1976.
- (5) U. Hornung, "A Numerical Method for the Simulation of Unsteady Groundwater Flow in Both Saturated and Unsaturated Soils," Soil Sci., Vol. 124, 1977, 140-144.
- (6) P. A. Witherspoon, et al., "Validity of Cubic Law for Fluid Flow in a Deformable Rock Fracture," Water Resources Research, Vol. 16, No. 6, 1980, 1016-1024.
- (7) R. van Genuchten, "Calculating the Unsaturated Hydraulic Conductivity With a New Closed-form Analytical Model," Water Resources Bulletin, Princeton University Press, 1978.
- (8) Y. Mualem, "A New Model for Predicting the Hydraulic Conductivity of Unsaturated Porous Media," Water Resources Research, Vol. 12, No. 3, 1976.
- (9) J. R. Philip, "The Theory of Infiltration: 1. The Infiltration Equation and Its Solution," Soil Sci., Vol. 83, 1957, 345-357.
- (10) R. H. Nilson, "Transient Two-Dimensional Diffusion Along a High-Diffusivity Lamina Which Bisects a Half-Space," Jour. of Eng. Math., Vol. 14, 1980, 263-282.
- (11) S. K. Griffiths, private communication, Sandia National Laboratories, Albuquerque, NM, 1984.
- (12) K. H. Haskell, W. H. Vandevender, E. L. Walton, "The SLATEC Common Mathematical Subprogram Library: SNLA Implementation," SAND80-2792, Sandia National Laboratories, Albuquerque, NM, 1980.
- (13) E. W. Washburn, "The Dynamics of Capillary Flow," Phys. Rev., Vol. 17, 1921, 273-283.
- (14) J. B. Walsh, "Effect of Pore Pressure and Confining Pressure on Fracture Permeability," Int. J. Rock Mech. Min. Sci. and Geomech. Abstr., Vol. 18, 1981, 429-435.

- (15) R. R. Peters, E. A. Klavetter, I. J. Hall, S. C. Blair, P. R. Heller, and G. W. Gee, "Fracture and Matrix Hydrologic Characteristics of Tuffaceous Materials from Yucca Mountain, Nye County, Nevada," SAND84-1471, Sandia National Laboratories, Albuquerque, NM, 1984.
- (16) B. A. Finlayson, "Water Movement in Desiccated Soils," In Proceedings of the First International Conference on Finite Elements in Water Resources, 3.91-3.106, Pentech Press, Plymouth, England.
- (17) R. A. Freeze, "The Mechanism of Natural Groundwater Recharge and Discharge: 1. One-Dimensional, Vertical, Unsteady, Unsaturated Flow Above a Recharging or Discharging Groundwater Flow System," Water Resources Research, Vol. 5, 1969, 153-171.
- (18) E. A. Klavetter and R. R. Peters, "Estimation of Hydrologic Properties of An Unsaturated, Fractured Rock Mass," SAND84-2642, Sandia National Laboratories, Albuquerque, NM, 1986.

APPENDIX A

The method of lines technique involves discretizing spatial terms by finite differences and results in a set of N ordinary differential equations in time. N is the number of node points in the grid. Combining (1) and (2) and applying finite differences to spatial terms results in the following set of ODEs.

$$\frac{d\psi_i}{dt} = \frac{1}{\left(\frac{d\theta}{d\psi}\right)_i} \left\{ \frac{1}{\Delta x} \left[K_{i+1/2} \left(\frac{\psi_{i+1} - \psi_i}{\Delta x} \right) - K_{i-1/2} \left(\frac{\psi_i - \psi_{i-1}}{\Delta x} \right) - \frac{1}{2} (K_{i+1} - K_{i-1}) \right] - Q_i \right\}, \quad i = 1, \dots, N$$

where

$$K_{i+1/2} = \frac{K_{i+1} + K_i}{2} \quad ; \quad K_{i-1/2} = \frac{K_i + K_{i-1}}{2}$$

and

- i - node index
- K - hydraulic conductivity for the fracture, (L/T)
- Q - seepage loss to matrix, $Q = 2V_w/w$, (1/T)
- t - time, (T)
- Δx - spatial increment (L)
- ψ - pressure head (L)
- θ - moisture content in the fracture (L^3/L^3)
- $\frac{d\theta}{d\psi}$ - moisture capacitance (1/L)

APPENDIX B

This Appendix contains a list of parameters used in this study and the corresponding values from the NNWSI Project Reference Information Base (RIB). These analyses were completed before Version 01.001 of the RIB was issued. This report does not contain any data that should be included in the NNWSI Project Site and Engineering Properties Data Base (SEPDB).

COMPARISON OF DATA USED IN THIS REPORT (SAND 84-1697) WITH DATA IN RIB VERSION 01.001

Parameter	Unit	Author's Value	RIB Value	RIB Subsection	Remarks
Ambient Saturation	TCw	.25 - .90	None	1.1.3.1	Parameter being varied for a parametric study
	PTn	.15 - .90	None		
	TSw2	.25 - .90	.85 ± .19		
	CHnz	.15 - .90	.91 ± .06		
	CHnv	.15 - .90	.90		
Residual Saturation	TCw	.04	None	1.1.3.2	
	PTn	.1178	None		
	TSw2	.0669	.091 ± .092		
	CHnz	.0809	.121 ± .067		
	CHnv	.0747	.085 ± .066		
Matrix a (van Genuchten parameter)	TCw	.144 x 10 ⁻³	None	1.1.4.1	
	PTn	.151 x 10 ⁻³	None		
	TSw2	.519 x 10 ⁻⁴	None		
	CHnz	.365 x 10 ⁻⁴	None		
	CHnv	.890 x 10 ⁻⁴	None		
Matrix b (van Genuchten parameter)	TCw	1.470	None	1.1.4.1	
	PTn	6.866	None		
	TSw2	1.787	None		
	CHnz	1.489	None		
	CHnv	5.862	None		
Saturated Matrix Hydraulic Conductivity, K _m (mm/yr)	TCw	0.41	None	1.1.4.2	
	PTn	12,307.	None		
	TSw2	0.60	.722		
	CHnz	0.63	(0.128 - 4.073) .535		
	CHnv	8,520.	(0.037 - 7.648) 107.2 (1.886 - 6089.9)		
Matrix Porosity	TCw	.07	None	1.1.8.1	
	PTn	.41	None		
	TSw2	.094	.106 ± .046		
	CHnz	.33	.269 ± .047		
	CHnv	.42	.324 ± .088		
Fracture Aperture (μm)	TCw	25 - 100	None	1.3.2.4.2.3	Parameter being varied for a parametric study
	PTn	25 - 100	None		
	TSw2	25 - 100	None		
	CHnz	25 - 100	None		
	CHnv	25 - 100	None		

DISTRIBUTION LIST

C. E. Kay, Acting Director (RW-1)
Office of Civilian Radioactive
Waste Management
U.S. Department of Energy
Forrestal Bldg.
Washington, D.C. 20585

Ralph Stein (RW-30)
Office of Civilian Radioactive
Waste Management
U.S. Department of Energy
Forrestal Bldg.
Washington, D.C. 20585

M. W. Frei (RW-22)
Office of Civilian Radioactive
Waste Management
U.S. Department of Energy
Forrestal Bldg.
Washington, D.C. 20585

B. G. Gale (RW-23)
Office of Civilian Radioactive
Waste Management
U.S. Department of Energy
Forrestal Bldg.
Washington, D.C. 20585

Samuel Rousso (RW-10)
Office of Civilian Radioactive
Waste Management
U.S. Department of Energy
Forrestal Bldg.
Washington, D.C. 20585

J. D. Saltzman (RW-20)
Office of Civilian Radioactive
Waste Management
U.S. Department of Energy
Forrestal Bldg.
Washington, D.C. 20585

S. J. Brocoum (RW-221)
Office of Civilian Radioactive
Waste Management
U.S. Department of Energy
Forrestal Building
Washington, D.C. 20585

V. J. Cassella (RW-123)
Office of Civilian Radioactive
Waste Management
U.S. Department of Energy
Forrestal Bldg.
Washington, D.C. 20585

S. H. Kale (RW-20)
Office of Civilian Radioactive
Waste Management
U.S. Department of Energy
Forrestal Bldg.
Washington, D.C. 20585

T. H. Isaacs (RW-40)
Office of Civilian Radioactive
Waste Management
U.S. Department of Energy
Forrestal Bldg.
Washington, D.C. 20585

D. H. Alexander (RW-332)
Office of Civilian Radioactive
Waste Management
U.S. Department of Energy
Forrestal Bldg.
Washington, D.C. 20585

C. Bresee (RW-10)
Office of Civilian Radioactive
Waste Management
U.S. Department of Energy
Forrestal Bldg.
Washington, D.C. 20585

Gerald Parker (RW-333)
Office of Civilian Radioactive
Waste Management
U.S. Department of Energy
Forrestal Bldg.
Washington, D.C. 20585

Chief, Repository Projects Branch
Division of Waste Management
U.S. Nuclear Regulatory Commission
Washington, D.C. 20555

NTS Section Leader
Repository Project Branch
Division of Waste Management
U.S. Nuclear Regulatory Commission
Washington, D.C. 20555

Document Control Center
Division of Waste Management
U.S. Nuclear Regulatory Commission
Washington, D.C. 20555

Carl P. Gertz, Project Manager (6)
Waste Management Project Office
U.S. Department of Energy
Nevada Operations Office
P.O. Box 98518
Mail Stop 523
Las Vegas, NV 89193-8518

J. L. Fogg (12)
Technical Information office
Nevada Operations Office
U. S. Department of Energy
P.O. Box 98518
Las Vegas, NV 89193-8518

C. L. West, Director
Office of External Affairs
U.S. Department of Energy
Nevada Operations Office
P.O. Box 98518
Las Vegas, NV 89193-8518

W. M. Hewitt, Program Manager
Roy F. Weston, Inc.
955 L'Enfant Plaza, Southwest
Suite 800
Washington, D.C. 20024

Technical Information Center
Roy F. Weston, Inc.
955 L'Enfant Plaza, Southwest
Suite 800
Washington, D.C. 20024

L. D. Ramspott (3)
Technical Project Officer for NNWSI
Lawrence Livermore National
Laboratory
P.O. Box 808
Mail Stop L-204
Livermore, CA 94550

M. E. Spaeth
Technical Project Officer for NNWSI
Science Applications International
Corp.
101 Convention Center Dr.
Suite 407
Las Vegas, NV 89109

H. N. Kalia
Exploratory Shaft Test Manager
Los Alamos National Laboratory
Mail Stop 527
101 Convention Center Dr.
Suite P230
Las Vegas, NV 89109

D. T. Oakley (4)
Technical Project Officer for NNWSI
Los Alamos National Laboratory
P.O. Box 1663
N-5, Mail Stop J521
Los Alamos, NM 87545

L. R. Hayes (6)
Technical Project Officer for NNWSI
U.S. Geological Survey
P.O. Box 25046
421 Federal Center
Denver, CO 80225

Center for Nuclear Waste
Regulatory Analyses
6220 Culebra Road
Drawer 28510
San Antonio, TX 78284

R. L. Bullock
Technical Project Officer for NNWSI
Fenix & Scisson, Inc.
101 Convention Center Dr.
Suite 320
Mail Stop 403
Las Vegas, NV 89109-3265

James C. Calovini
Technical Project Officer for NNWSI
Holmes & Narver, Inc.
101 Convention Center Dr.
Suite 860
Las Vegas, NV 89109

Dr. David W. Harris
NNWSI Technical Project Officer
Bureau of Reclamation
P.O. Box 25007 Bldg. 67
Denver Federal Center
Denver, CO 80225-0007

M. D. Voegele
Science Applications International
Corp.
101 Convention Center Dr.
Suite 407
Las Vegas, NV 89109

J. A. Cross, Manager
Las Vegas Branch
Fenix & Scisson, Inc.
P.O. Box 93265
Mail Stop 514
Las Vegas, NV 89193-3265

P. T. Prestholt
NRC Site Representative
1050 East Flamingo Road
Suite 319
Las Vegas, NV 89119

A. E. Gurrola, General Manager
Energy Support Division
Holmes & Narver, Inc.
P.O. Box 93838
Mail Stop 580
Las Vegas, NV 89193-3838

B. L. Fraser, General Manager
Reynolds Electrical & Engineering Co.
P.O. Box 98521
Mail Stop 555
Las Vegas, NV 89193-8521

P. K. Fitzsimmons, Director
Health Physics & Environmental
Division
Nevada Operations Office
U.S. Department of Energy
P.O. Box 98518
Las Vegas, NV 89193-8518

Robert F. Pritchett
Technical Project Officer for NNWSI
Reynolds Electrical & Engineering Co.
P.O. Box 98521
Mail Stop 615
Las Vegas, NV 89193-8521

Elaine Ezra
NNWSI GIS Project Manager
EG&G Energy Measurements, Inc.
P.O. Box 1912
Mail Stop H-02
Las Vegas, NV 89125

SAIC-T&MSS Library (2)
Science Applications International
Corp.
101 Convention Center Dr.
Suite 407
Las Vegas, NV 89109

Dr. Martin Mifflin
Desert Research Institute
Water Resources Center
2505 Chandler Avenue
Suite 1
Las Vegas, NV 89120

E. P. Binnall
Field Systems Group Leader
Building 50B/4235
Lawrence Berkeley Laboratory
Berkeley, CA 94720

T. G. Barbour
Science Applications International
Corp.
1626 Cole Blvd., Suite 270
Golden, CO 80401

V. M. Glanzman
U.S. Geological Survey
P.O. Box 25046
913 Federal Center
Denver, CO 80225

C. H. Johnson
Technical Program Manager
Nuclear Waste Project Office
State of Nevada
Evergreen Center, Suite 252
1802 North Carson Street
Carson City, NV 89710

T. Hay, Executive Assistant
Office of the Governor
State of Nevada
Capitol Complex
Carson City, NV 89710

R. R. Loux, Jr., (3)
Executive Director
Nuclear Waste Project Office
State of Nevada
Evergreen Center, Suite 252
1802 North Carson Street
Carson City, NV 89710

John Fordham
Desert Research Institute
Water Resources Center
P.O. Box 60220
Reno, NV 89506

Prof. S. W. Dickson
Department of Geological Sciences
Mackay School of Mines
University of Nevada
Reno, NV 89557

J. R. Rollo
Deputy Assistant Director for
Engineering Geology
U.S. Geological Survey
106 National Center
12201 Sunrise Valley Dr.
Reston, VA 22092

Eric Anderson
Mountain West Research-Southwest
Inc.
Phoenix Gateway Center
432 North 44 Street
Suite 400
Phoenix, AZ 85008-6572

Judy Foremaster (5)
City of Caliente
P.O. Box 158
Caliente, NV 89008

A. T. Tamura
Science and Technology Division
Office of Scientific and Technical
Information
U.S. Department of Energy
P.O. Box 62
Oak Ridge, TN 37831
Oak Ridge, TN 37831

L. Jardine
Project Manager
Bechtel National Inc.
P.O. Box 3965
San Francisco, CA 94119

R. Harig
Parsons Brinckerhoff Quade &
Douglas
1625 Van Ness Ave.
San Francisco, CA 94109-3679

Dr. Roger Kasperson
CENTED
Clark University
950 Main Street
Worcester, MA 01610

Robert E. Cummings
Engineers International, Inc.
P.O. Box 43817
Tucson, AZ 85733-3817

Dr. Jaak Daemen
Department of Mining and
Geotechnical Engineering
University of Arizona
Tucson, AZ 85721

Department of Comprehensive Planning
Clark County
225 Bridger Avenue, 7th Floor
Las Vegas, NV 89155

Economic Development Department
City of Las Vegas
400 East Stewart Avenue
Las Vegas, NV 89109

Planning Department
Nye County
P.O. Box 153
Tonopah, NV 89049

Director of Community Planning
City of Boulder City
P.O. Box 367
Boulder City, NV 89005

Commission of the European
Communities
200 Rue de la Loi
B-1049 Brussels
Belgium

Lincoln County Commission
Lincoln County
P.O. Box 90
Pioche, NV 89043

Community Planning & Development
City of North Las Vegas
P.O. Box 4086
North Las Vegas, NV 89030

ONWI Library
Battelle Columbus Laboratory
Office of Nuclear Waste Isolation
505 King Avenue
Columbus, OH 43201

T. N. Narisimhan
Lawrence Berkeley Laboratory
University of California
Berkeley, CA 94720

Prof. M. B. Fiering
Division of Applied Sciences
Harvard University
Cambridge, MA 02138

P. A. Witherspoon
Lawrence Berkeley Laboratory
University of California
Berkeley, CA 94720

B. Ross
GEOTRANS
11999 Katy Freeway, Suite 170
Houston, TX 77079

Professor K. S. Udell
Dept. of Mechanical Engineering
University of California
Berkeley, CA 94720

T. R. Pigford
Dept. of Nuclear Engineering
University of California
Berkeley, CA 94720

City Manager
City of Henderson
Henderson, NV 89015

Librarian
Los Alamos Technical
Associates, Inc.
P.O. Box 410
Los Alamos, NM 87544

1510 J. W. Nunziato
1511 D. K. Gartling
1511 N. E. Bixler
1511 R. R. Eaton
1511 P. Hopkins
1511 M. J. Martinez (10)
1511 D. F. McTigue
1512 J. C. Cummings
1513 D. W. Larson
1513 R. C. Dykhuizen
1520 L. W. Davison
1530 W. Herrmann, Actg.
1550 C. W. Peterson
6300 R. W. Lynch
6310 T. O. Hunter
6310 NNWSICF
6310 72-12141-0/QIII
6310 100/12144/SAND84-1697/Q3
6311 A. L. Stevens
6311 C. Mora
6312 F. W. Bingham
6312 G. E. Barr
6312 A. L. Dudley
6312 J. Gauthier
6312 R. R. Peters
6312 R. W. Prindle
6312 M. S. Tierney
6313 T. E. Blejwas
6313 E. A. Klavetter
6313 F. B. Nimick
6313 B. M. Schwartz
6313 R. M. Zimmerman
6314 J. R. Tillerson
6314 J. A. Fernandez
6315 T. O. Hunter, Actg.
6316 R. P. Sandoval
6317 S. Sinnock
6330 W. D. Weart
6332 WMT Library (20)
6334 D. R. Anderson
6410 N. R. Ortiz
6431 R. M. Cranwell
8024 P. W. Dean
8316 J. Lipkin
3141 S. A. Landenberger (5)
3151 W. Klein
3154-3 C. H. Dalin (8)
for DOE/OSTI

